

# A Quantum Chemistry Study for Ionic Liquids Applied to Gas Capture and Separation

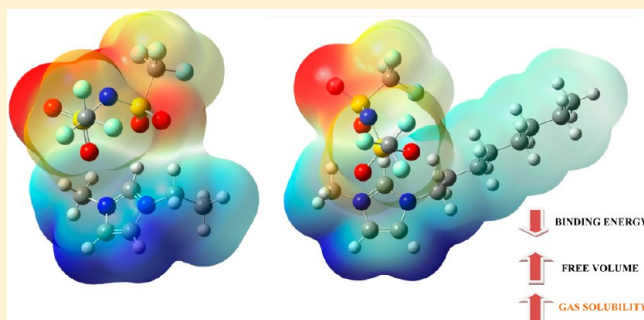
Giane B. Damas,<sup>†</sup> Amina B. A. Dias,<sup>†</sup> and Luciano T. Costa<sup>\*,‡</sup>

<sup>†</sup>Instituto de Química, Universidade Federal de Alfenas - Rua Gabriel Monteiro da Silva, 700 Alfenas – MG, CEP:37130-000, Brazil

<sup>‡</sup>Instituto de Química, Universidade Federal Fluminense - Outeiro de São João Batista s/n Niterói –RJ, CEP:20150-020, Brazil

## S Supporting Information

**ABSTRACT:** In recent years, the global climate change is in evidence and it is almost a consensus that it is caused by the greenhouse gases emissions. An alternative to reduce these emissions is carbon capture and storage (CCS), which employs solvents based on amine compounds. In this scene, ionic liquids (IL) have been investigated to a greater extent for this application. In this work, we make an evaluation of interactions between gases ( $\text{CO}_2$ ,  $\text{SO}_2$ , and  $\text{H}_2\text{S}$ ) and anion/cation from IL, as well as cation–anion interactions. For this, quantum calculations under vacuum were performed at the B3LYP/6-311+G\*\* level of theory and using the M06-2X functional, where dispersion effects are considered. Among the well-studied systems based on imidazolium cations and fluorinated anions, we also studied the tetraalkylammonium, tetraalkylphosphonium, ether-functionalized imidazolium based systems, and tetrahexylammonium bis(trifluoromethanesulfonyl)imide,  $[\text{THA}][\text{Tf}_2\text{N}]$ , as a potential prototype. The ion pairs evaluated include  $[\text{Tf}_2\text{N}]^-$ -based IL, with alkyl chain varying from  $[\text{C}_1\text{mim}]^+$  to  $[\text{C}_8\text{mim}]^+$  and  $[\text{C}_1\text{mim}]^+$ -based IL. We found that the anion becomes more available to interact with gas with the weakening of the cation–anion interaction.  $[\text{THA}][\text{Tf}_2\text{N}]$  has a binding energy of  $-274.89$  kJ/mol at the B3LYP/6-311+G\*\* level of theory, which is considered energetically interesting to gas capture applications.



## ■ INTRODUCTION

Although global warming is not a consensus by the scientific community we can see every day probes that it is occurring. Since last century the global air and sea temperature surface has increased about  $0.8^\circ\text{C}$ . On the other hand, it is almost a consensus that the greenhouse gases emissions are responsible for global climate changes. We can state the emissions of greenhouse gases due to human activities have been documented as well as the effects on global warming resulting from it. Efforts to reduce greenhouse gases at the source are crucial to curb climate change, but due to insignificant economic incentives to reduce usage of fossil fuels not a lot of progress has been made by this route. According to the Intergovernmental Panel on Climate Change (IPCC) global emissions are 60% higher than at the time of the first IPCC report in 1990, with a 200 billion tonnes of  $\text{CO}_2$  being released into the atmosphere. On the other hand, fossil fuels are cheaper than most other alternatives; however, the price of fossil energy does not consider the cost of dealing with climate change.<sup>1,2</sup>

Many experimental<sup>3–11</sup> and theoretical<sup>12–19</sup> works have been dedicated to the carbon capture and storage (CCS) problem.<sup>20,21</sup> In this sense, ionic liquids (ILs) have been used as low volatility “green” solvents, but other favorable properties such as thermal stability, the wide range of electrochemical windows, good ionic conductivity, low flammability and corrosivity, and very low vapor pressure<sup>22</sup> have stimulated researchers to consider ILs as

multipurpose advanced materials.<sup>23</sup> In fact, Ionic Liquids are being investigated in many different kinds of systems since there are fundamental purposes to technology applications. However, we can state that fewer studies have become useful even though they have contributed to the understanding of Ionic Liquids physical chemistry. For instance, we have been the first group that carried out molecular dynamics (MD) simulations of the ionic liquids polymer electrolytes.<sup>24,25</sup> In these studies, the local environment around the cations in MD simulations was confirmed by density functional theory (DFT) calculations and this level of theory was able to give good agreement with the Raman spectroscopy measurements data.<sup>26</sup> It is known that ionic liquids present a high capacity to solvate a wide variety of compounds. From the first works exploring the use of ILs as a potential candidate to capture  $\text{CO}_2$  we have seen two main scientific discussions about the important role of the anions and the free volume as the most important features in  $\text{CO}_2$  capture by the ILs systems. Cadena et al. were one of the first to probe that the anion plays an important role in  $\text{CO}_2$  solubility.<sup>3</sup> Following that many other investigations have been dedicated to understand how the anions are contributing to the high  $\text{CO}_2$  solubility in ILs and the free volume effect on the  $\text{CO}_2$  capture as

Received: April 3, 2014

Revised: June 28, 2014

Published: July 2, 2014

well.<sup>2,14,27–29</sup> Bhargava et al. used density functional theory calculations in the gas phase to obtain the binding energy for many clusters (CO<sub>2</sub>-anion), from halogen ion to bis-(trifluoromethanesulphonyl)imide ([N(CF<sub>3</sub>SO<sub>2</sub>)<sub>2</sub>]<sup>−</sup>).<sup>14</sup> They described the optimized geometries which yielded a Lewis acid–base type of interaction between CO<sub>2</sub> and the anions, the strength of which was found to be directly proportional to the basicity of the anion. One of the most important results was related to the calculated binding energies, which were inversely proportional to the solubility of CO<sub>2</sub> in ILs. Other studies have explored the Lewis acid/Lewis base interaction between CO<sub>2</sub> and ionic liquids<sup>30,31</sup> but few works have investigated the mechanism of solvation in-depth and the correlation between anion/cation interactions as well. We know the ionic liquids present a molecular architecture that allows one to change atoms or functional groups to modulate their properties, enabling the design of new functional materials, while retaining the desired main core features of an IL.<sup>32</sup> For instance, Bara et al. demonstrated that some ILs exhibit preferred absorption of certain gases, which is an important property to be applied for the gas-separation process.<sup>33</sup> These functionalized ILs have a remarkable feature and they are also being investigated as potential absorbents for CO<sub>2</sub> capture. Goodrich et al. have studied the influence of the amine-functionalized anion and the length of the alkyl chain in tetraalkylphosphonium derived ILs. They also have demonstrated that after the CO<sub>2</sub> chemical absorption the viscosity increased suddenly, probably due to the formation of a hydrogen bonding network.<sup>33</sup> Siqueira et al. carried out MD simulations of tunable ionic liquids showing that change of the structure of the cation can also modulate the dynamic properties, such as viscosity.<sup>34</sup> In recent work, we have used both MD simulations and quantum chemistry calculations to discuss more deeply the mechanisms that are involved with the CO<sub>2</sub> solubility in ILs.<sup>35</sup> These four studies were performed for the 1-ethyl-3-methylimidazolium (C<sub>2</sub>mim<sup>+</sup>) and bis(trifluorosulfonyl)imide (Tf<sub>2</sub>N)<sup>−</sup> which is one of the most investigated systems for CO<sub>2</sub> capture.<sup>35</sup> However, we can consider that there is a lack of the systematic quantum chemistry study exploring different kinds of tools to investigate ionic liquids derived cations and anions as well as their interaction with CO<sub>2</sub>, SO<sub>2</sub>, and H<sub>2</sub>S. In this sense, in the current paper we aim to study the mechanisms of the interactions that occur between ionic liquids and gases, evaluating its strength through binding energy calculations and AIM (quantum theory of atoms in molecules) analysis, as well as correlating with solubility data reported in the literature.

In this work, quantum calculations were performed at the B3LYP/6-311+G\*\* level of theory to verify the geometrical parameters after interaction between cation–gas and anion–gas including the imidazolium and imidazolium-functionalized cations series and alkylsulfate series in the first step. Then, we establish the energetic contribution to solubility considering [Tf<sub>2</sub>N]<sup>−</sup>-based IL and varying the cation in the series of imidazolium and imidazolium-functionalized cations. Further, we evaluate the interaction between gas and ion pairs. Dispersion effects were analyzed through calculations by using the M06-2X functional and finally we develop a novel ionic pair, based on our results.

## METHODOLOGY

**Simulation Details.** All molecular models used in this work were built by using the Avogadro package.<sup>36</sup> The work was divided into two parts, consisting of quantum chemistry calculations of cation–gas and anion–gas interactions (Part I),

cation–anion and ion pair–gas interactions (Part II) in vacuum. These systems are described in Table 1. This part was dedicated to get the optimized geometry and the binding energy to evaluate the strength of these interactions. So, it is possible to establish the influence of ion nature on gas-IL interactions as well as make an appropriate combination of cation and anions in order to get an IL with good features to be applied in the absorption process.<sup>27</sup> For each ion–gas calculation, we used at least eight different starting configurations and for the ion pairs, at least four starting ones to explore better the potential energy surface (PES). The gases are CO<sub>2</sub>, SO<sub>2</sub>, and H<sub>2</sub>S. In the ion pair–gas calculations, we considered only CO<sub>2</sub> and the ion pairs coordinates were frozen from [C<sub>3</sub>mim][Tf<sub>2</sub>N]CO<sub>2</sub> systems to [C<sub>8</sub>mim][Tf<sub>2</sub>N]CO<sub>2</sub>, based on the fact that CO<sub>2</sub> is not capable of modifying the ion pair structure.<sup>2,35</sup> Furthermore, the electronic energy was not modified significantly with frozen coordinates, but the computational cost is reduced drastically. Finally, we present results related to the [THA][Tf<sub>2</sub>N] ion pair.

The DFT method with the Becke's three-parameter functional and the nonlocal correlation of Lee, Yang, and Parr (B3LYP)<sup>37</sup> together with the 6-311+G(d,p) basis set<sup>38</sup> were used for all calculations. We need to highlight previous studies have demonstrated that the DFT method is suitable for calculation of ILs.<sup>14,39–41</sup> We also have previously carried out studies on ILs using this level of theory and good agreement to the experimental data was found.<sup>24,26</sup> Vibration frequencies were calculated at the same level of theory to confirm the minimum state in PES.

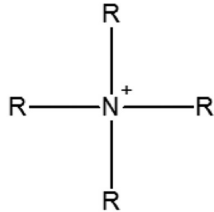
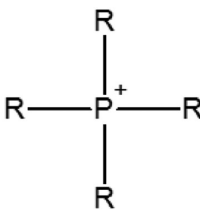
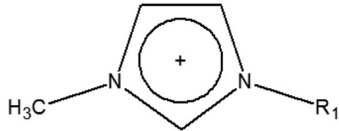
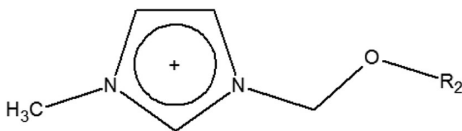
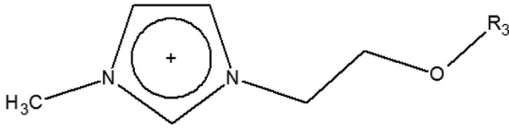
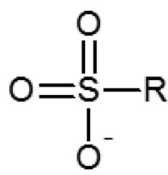
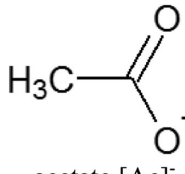
According to Izgorodina et al.<sup>42</sup> the presence of extended alkyl chains in cations from ILs results in nanoscale segregation, where nonpolar domains are controlled by dispersive forces, the contributions from these forces in the equilibrium structure and the binding/interaction energies becoming significant. These effects were considered in our calculations by using Truhlar's M06-2X functional<sup>43</sup> with the same basis set (6-311+G\*\*) for imidazolium-based and imidazolium functionalized-based systems. Partial charges and electrostatical potential surfaces (EPS) were calculated through populational analysis and visualized in the GaussView 05 interface.<sup>44</sup> Quantum chemistry calculations were performed with the Gaussian 09 program.<sup>45</sup>

Another tool employed to measure the interaction strength was the AIM analysis by means of the AIMAll software.<sup>46</sup> In this tool, there is one bond critical point (BCP) between each pair of atoms bonded or interacting, where a critical point is defined by the point localized between two attractors. The electron density associated with all critical points ( $\rho_{\text{total}}$ ) involved in the interaction is correlated to its strength. On the other hand, the Laplacian of the density ( $\nabla^2\rho$ ) indicates regions with concentration of local charge and presents a negative sign when a bond occurs, and a positive one defining a weak interaction.<sup>47</sup>

## RESULTS AND DISCUSSION

**Cation–Gas Interactions.** Table 2 shows results for cation–CO<sub>2</sub> interactions obtained at the B3LYP level, in which  $E_0$ +ZPE is related to the electronic energy ( $E_0$ ) with zero-point energy (ZPE) correction,  $\Delta E_{\text{CP}}$  (kJ/mol) is the binding energy with correction of basis set superposition error (BSSE) by means of the counterpoise method. The parameters  $d_1$  and  $d_2$  express the gas bond lengths after interaction with the cation. For CO<sub>2</sub> and SO<sub>2</sub>,  $d_2$  is either C–O or S–O involved in the interaction (Figure 1), while  $d_1$  is the C–O bond length not involved with the intermolecular interaction with the cation. The results for SO<sub>2</sub> and H<sub>2</sub>S molecules are shown in the Supporting Information, Table S1.

Table 1. Structural Formula of the Chemical Compounds Studied in This Work<sup>a</sup>

Ion-Gas Systems (CO <sub>2</sub> , SO <sub>2</sub> and H <sub>2</sub> S)	
<i>Cations</i>	
<i>Tetraalkylammonium and Tetraalkylphosphonium groups</i>	
	
-CH <sub>3</sub> , tetramethylammonium [TMA] <sup>+</sup> -C <sub>2</sub> H <sub>5</sub> , tetraethylammonium [TEA] <sup>+</sup> -C <sub>4</sub> H <sub>9</sub> , tetrabutylammonium [TBA] <sup>+</sup> -C <sub>6</sub> H <sub>11</sub> , tetrahexylammonium [THA] <sup>+</sup>	R=-CH <sub>3</sub> , tetramethylphosphonium [TMF] <sup>+</sup> -C <sub>2</sub> H <sub>5</sub> , tetraethylphosphonium [TEF] <sup>+</sup> -C <sub>4</sub> H <sub>9</sub> , tetrabutylphosphonium [TBF] <sup>+</sup> -C <sub>6</sub> H <sub>11</sub> , tetrahexylphosphonium [THF] <sup>+</sup> -H, [phosphonium] <sup>+</sup>
<i>Imidazolium Series</i>	
	R <sub>1</sub> =-CH <sub>2</sub> , dimethylimidazolium [C <sub>1</sub> mim] <sup>+</sup> -CH <sub>2</sub> CH <sub>3</sub> , 1-ethyl-3-methyl-imidazolium [C <sub>2</sub> mim] <sup>+</sup> -C <sub>3</sub> H <sub>7</sub> , 1-propyl-3-methyl-imidazolium [C <sub>3</sub> mim] <sup>+</sup> -C <sub>4</sub> H <sub>9</sub> , 1-butyl-3-methyl-imidazolium [C <sub>4</sub> mim] <sup>+</sup> -C <sub>5</sub> H <sub>11</sub> , 1-pentyl-3-methyl-imidazolium [C <sub>5</sub> mim] <sup>+</sup> -C <sub>6</sub> H <sub>13</sub> , 1-hexyl-3-methyl-imidazolium [C <sub>6</sub> mim] <sup>+</sup> -C <sub>8</sub> H <sub>17</sub> , 1-octyl-3-methyl-imidazolium [C <sub>8</sub> mim] <sup>+</sup>
<i>Ether Functionalized-Imidazolium series</i>	
	R <sub>2</sub> = -CH <sub>3</sub> , 1-methoxy-methyl-3-methyl-imidazolium [C <sub>1</sub> Odmim] <sup>+</sup> -C <sub>3</sub> H <sub>6</sub> OCH <sub>3</sub> , 1-methoxy-trioxy-methyl-3-methyl-imidazolium [C <sub>1</sub> OC <sub>3</sub> Odmim] <sup>+</sup> -C <sub>2</sub> H <sub>4</sub> OCH <sub>3</sub> , 1-methoxy-dioxy-methyl-3-methyl-imidazolium [C <sub>1</sub> OC <sub>2</sub> Odmim] <sup>+</sup>
	R <sub>3</sub> = -C <sub>2</sub> H <sub>4</sub> OCH <sub>3</sub> , 1-methoxy-dioxy-ethyl-3-methylimidazolium [C <sub>1</sub> OC <sub>2</sub> Oemim] <sup>+</sup> -CH <sub>3</sub> , 1-methoxy-ethyl-3-methyl-imidazolium [C <sub>1</sub> Oemim] <sup>+</sup>
<i>Anions</i>	
<i>Alkylsulfate Group and Acetate</i>	
	
R= -O, sulfate [SO <sub>4</sub> ] <sup>2-</sup> -OCH <sub>3</sub> , methylsulfate [MeSO <sub>4</sub> ] <sup>-</sup> -OCH <sub>2</sub> CH <sub>3</sub> , ethylsulfate [EtSO <sub>4</sub> ] <sup>-</sup> -OCH <sub>2</sub> CH <sub>2</sub> CH <sub>2</sub> CH <sub>3</sub> , butylsulfate [BuSO <sub>4</sub> ] <sup>-</sup>	-acetate [Ac] <sup>-</sup>

<sup>a</sup>Cations, with imidazolium, imidazolium-functionalized, tetraalkylammonium, and tetraalkylphosphonium series; anions, with halide, fluorinated, alkylsulfate groups, and acetate; [C<sub>1</sub>mim]-based ionic pairs; [Tf<sub>2</sub>N]<sup>-</sup>-based ionic pairs, considering imidazolium and imidazolium-functionalized series without and with gas.



**Table 2.** Data Obtained from Electronic Calculations for Cation-CO<sub>2</sub> Systems at the B3LYP/6-311+G\*\* Level of Theory<sup>a</sup>

cation-CO <sub>2</sub>	$E_0$ +ZPE (hartrees)	$\Delta E_{CP}$ (kJ/mol)	$d_1$ (Å)	$d_2$ (Å)
[TMA] <sup>+</sup>	-402.7001	-14.70	1.153	1.169
[TEA] <sup>+</sup>	-559.8834	-10.96	1.154	1.168
[TBA] <sup>+</sup>	-874.2527	-7.35	1.155	1.167
[THA] <sup>+</sup>	-1188.6206	-6.47	1.156	1.166
[phosphonium] <sup>+</sup>	-532.0896	-28.05	1.150	1.172
[TMF] <sup>+</sup>	-689.3702	-13.98	1.153	1.169
[TEF] <sup>+</sup>	-846.5477	-9.32	1.155	1.167
[TBF] <sup>+</sup>	-1160.9170	-8.22	1.155	1.167
[THF] <sup>+</sup>	-1475.2687	-7.99	1.155	1.167
[C <sub>1</sub> mim] <sup>+</sup>	-493.8080	-16.25	1.153	1.169
[C <sub>2</sub> mim] <sup>+</sup>	-533.1088	-14.91	1.153	1.168
[C <sub>3</sub> mim] <sup>+</sup>	-572.4051	-14.71	1.153	1.168
[C <sub>4</sub> mim] <sup>+</sup>	-611.7016	-14.62	1.153	1.168
[C <sub>5</sub> mim] <sup>+</sup>	-650.9980	-14.59	1.153	1.168
[C <sub>6</sub> mim] <sup>+</sup>	-690.2952	-14.77	1.153	1.168
[C <sub>8</sub> mim] <sup>+</sup>	-768.8870	-13.84	1.153	1.168
[C <sub>1</sub> Odmim] <sup>+</sup>	-608.3271	-11.55	1.154	1.168
[C <sub>1</sub> OC <sub>3</sub> Odmim] <sup>+</sup>	-801.4428	-12.91	1.154	1.167
[C <sub>1</sub> OC <sub>2</sub> Odmim] <sup>+</sup>	-762.1432	-14.27	1.153	1.168
[C <sub>1</sub> OC <sub>2</sub> Oemim] <sup>+</sup>	-801.4367	-15.03	1.153	1.168
[C <sub>1</sub> Oemim] <sup>+</sup>	-647.6231	-15.05	1.153	1.168

<sup>a</sup>Electronic energy with zero point correction ( $E_0$ +ZPE), binding energy with BSSE correction ( $\Delta E_{CP}$ ), and the CO<sub>2</sub> bond lengths ( $d_1$  and  $d_2$ ).

We can observe that the gas affinity decreases with an increase of cation size, as can be seen for the tetraalkylphosphonium series, where the binding energy is -13.98 kJ/mol for [TMF]<sup>+</sup>-CO<sub>2</sub> and -7.99 kJ/mol for [THF]<sup>+</sup>-CO<sub>2</sub>. This behavior occurred for all systems containing the three gases, except for [THA]<sup>+</sup>-SO<sub>2</sub>, whose binding energy increases in relation to [TBA]<sup>+</sup>-SO<sub>2</sub> (Table S1, Supporting Information). [THA]<sup>+</sup>-CO<sub>2</sub> has the lowest affinity among the cation-gas interactions, with  $\Delta E_{CP}$  = -6.47 kJ/mol. The negative values for all binding energies indicate the stability after the interaction.<sup>27</sup> The corrected electronic energy ( $E_0$ +ZPE) is an electron number functional<sup>48</sup> and becomes higher, in absolute terms, with the increasing of the atom number in the ion. In this case, the negative values are derived from the electron-nucleus attraction.

In general, the binding energy for the imidazolium series follows a tendency of decreasing with the alkyl chain. An exception is [C<sub>6</sub>mim]<sup>+</sup>, which presents higher affinity for CO<sub>2</sub> ( $\Delta E_{CP}$  = -14.77 kJ/mol) compared to [C<sub>5</sub>mim]<sup>+</sup> (-14.59 kJ/mol). In the case of ether functionalized-imidazolium group interacting with CO<sub>2</sub>, the highest binding energy is exhibited by [C<sub>1</sub>Oemim]<sup>+</sup>, -15.05 kJ/mol, which is almost equal to [C<sub>1</sub>OC<sub>2</sub>Oemim]<sup>+</sup>. In general, the ether group promotes a better distribution of charge in the nonpolar alkyl chain of imidazolium cation, whose carbon atoms nearby to the ring become less negative and allow the hydrogens to interact with the Lewis base. As a result, the interaction is stronger than equivalent nonfunctionalized imidazolium cations. The exception is [C<sub>1</sub>Odmim]<sup>+</sup>, which presents a interaction site near the C=C hydrogen, reducing its interaction strength. However, these effects are more evident when these cations interact with [Tf<sub>2</sub>N]<sup>-</sup>, which will be analyzed posteriorly.

The total electron density ( $\rho_{total}$ ) for the critical points related to imidazolium-based systems is shown in Table 3. For all

imidazolium-CO<sub>2</sub> systems  $\rho_{total}$  = 0.017 au, in good agreement with our previous MD simulations data for the [C<sub>2</sub>mim][Tf<sub>2</sub>N]-CO<sub>2</sub> system.<sup>35</sup> Due to the slight difference between the electron density of all systems, it is not possible to evaluate the alkyl effect over cation-gas interaction, using AIM. Table 4 describes  $\rho$  and  $\nabla^2\rho$  values over BCPs and RCPs for imidazolium-CO<sub>2</sub> cations.

These cations present weak interactions with CO<sub>2</sub>, as well as with SO<sub>2</sub> and H<sub>2</sub>S, which is indicated by the positive sign of  $\nabla^2\rho$  and  $\rho$  over BCPs lower than a covalent bond (over 0.02 au).<sup>35,47,49,50</sup> We can note that the interaction between O(gas)⋯H (bonded to C=N, as indicated by O19-H7 for [C<sub>1</sub>mim]<sup>+</sup> in Figure 2) becomes weaker with the increasing of the alkyl side chain, in which  $\rho$  ranges from 0.010183 au, in [C<sub>1</sub>mim]<sup>+</sup>-CO<sub>2</sub>, to 0.009539 au, in [C<sub>6</sub>mim]<sup>+</sup>-CO<sub>2</sub>. On the other hand, the interaction with the same oxygen and hydrogen from the cation methyl group (such as O19-H11 [C<sub>1</sub>mim]<sup>+</sup> in Figure 2) becomes stronger with the alkyl chain, except for [C<sub>5</sub>mim]<sup>+</sup>, with 0.003898 au (O31-H15). The RCP has the same behavior through the series. The cation-H⋯O interactions correspond to the H-bonds, as described by Popelier<sup>51</sup> ( $\rho$  = 0.002–0.035 au and  $\nabla^2\rho$  = 0.014–0.139 au).

For the cation-CO<sub>2</sub> systems, the interaction is not sufficient to produce a deviation from the CO<sub>2</sub> linear geometry.<sup>14</sup> It is particularly important to highlight that the broken CO<sub>2</sub> geometry is related to the possibility to convert it in other chemical row materials.<sup>52</sup> We have noted that for some systems, such as [TMA]<sup>+</sup>-CO<sub>2</sub>, the C-H bond is shortened by 0.001 Å with complexation, occasioned by the carbon radius increasing and consequent reduction of the H radius. As described by Grabowski,<sup>53</sup> this H-bond forming effect is valid for other Lewis acid-base systems. In the same way, there is stretching of  $d_2$  of C-O in interaction with cations, from 1.161 Å, in the isolated state, to 1.166 Å for [THA]<sup>+</sup> and 1.172 Å, for [phosphonium]<sup>+</sup> (Table 2). As a consequence,  $d_1$  decreases. There is a slightly tendency of  $d_2$  bond length increase with the binding energy while  $d_1$  distance decreases for the cation-CO<sub>2</sub> interactions (Figure 3). Stronger interactions weaken the C-O⋯H bond. Two optimized geometries are summarized in Figure 4 and other cation-gas systems are presented in Figure S1 in the Supporting Information.

The charge distribution over the CO<sub>2</sub> molecule in the [TMA]<sup>+</sup>-CO<sub>2</sub> can be visualized in the electrostatic potential map in Figure 5A while the  $\rho_{bcp}$  for the interaction sites between these system are shown in Figure 5B. We can note a negative charge concentration over O20, as indicated by the red color. The electron density at the bond critical points is slightly different with  $\rho_1$  = 0.465693 au and  $\rho_2$  = 0.448085 au. This is a probe of the charge transfer between the cation and gas, causing a stretching in the bond and changing the distribution of the electron cloud.

Considering isolated SO<sub>2</sub> in the gas phase, the optimized angle is 118.7°, with  $d_1$  =  $d_2$  = 1.458 Å. Unlike cation-CO<sub>2</sub> interactions, cation-SO<sub>2</sub> interactions present a distortion of this angle in the gas phase proportional to the binding energy, reaching 3.5° for [C<sub>1</sub>OC<sub>2</sub>Odmim]<sup>+</sup>-SO<sub>2</sub>. The fluctuation observed for the bond lengths occurs to the same extension compared to cation-CO<sub>2</sub> systems. For isolated H<sub>2</sub>S, in the gas phase, the optimized angle is equal to 92.5° and  $d_1$  =  $d_2$  = 1.348 Å. This angle is virtually not changed with the binding energy, due to the fact the interaction occurs with H<sub>2</sub>S negative dipole (sulfur) with the highest deviation observed of 1.5°, for [C<sub>1</sub>OC<sub>3</sub>Odmim]<sup>+</sup>-H<sub>2</sub>S. In the same way, there is not significant amendment in the H-S bond lengths, although cation-H<sub>2</sub>S interactions are hardest than those observed for cation-CO<sub>2</sub> systems.

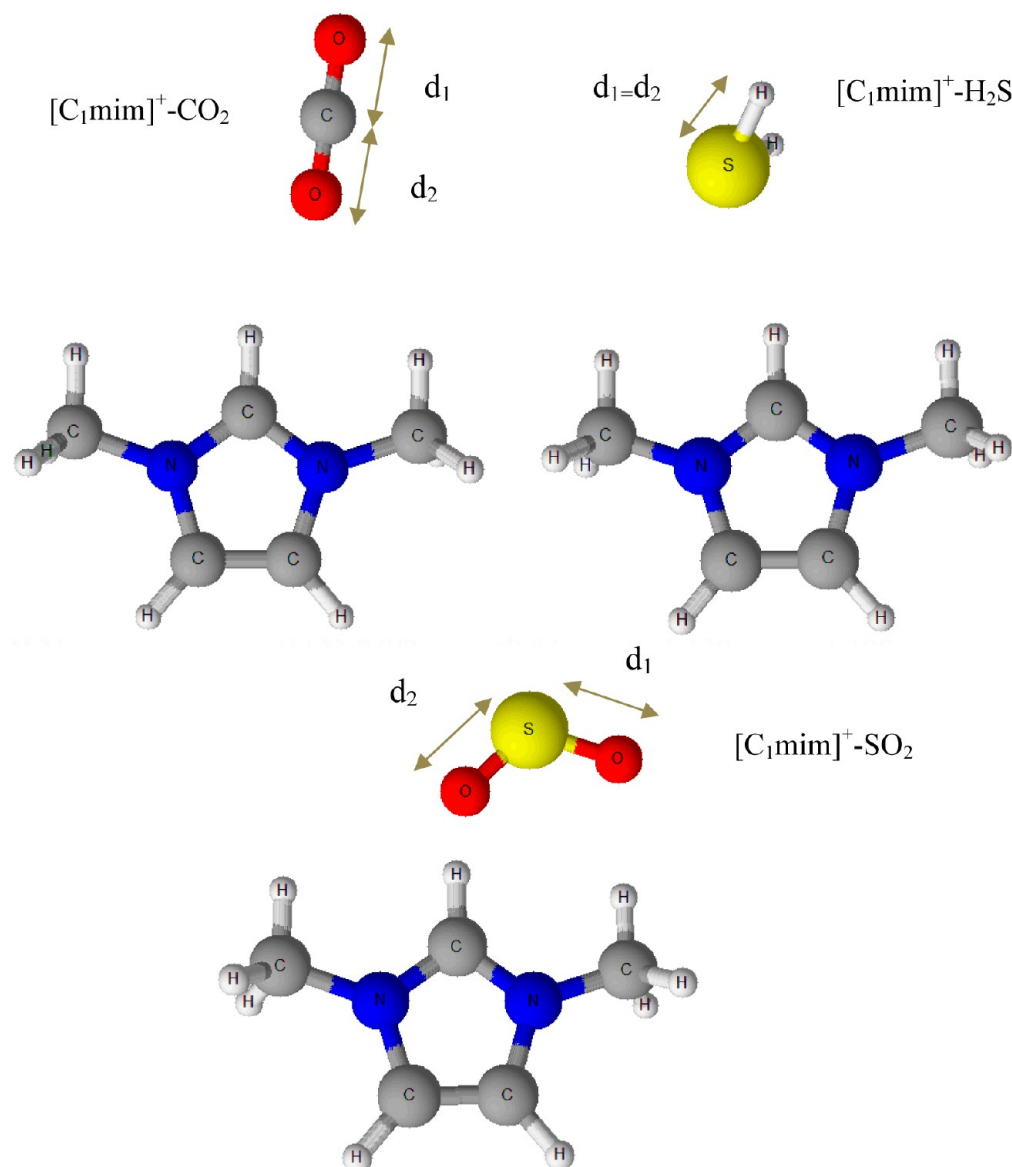


**Figure 1.** Schematic representation for the optimized geometries related to [C<sub>1</sub>mim]<sup>+</sup>-CO<sub>2</sub> and [C<sub>1</sub>mim]<sup>+</sup>-SO<sub>2</sub> interactions, showing the  $d_1$  and  $d_2$  parameters. The gray, red, blue, yellow, and white spheres represent carbon, oxygen, nitrogen, sulfur, and hydrogen atoms, respectively.

**Table 3. Total Electron Density ( $\rho_{\text{total}}$ ) in Interactions Sites of Cation–Gas Systems<sup>a</sup>**

system	$\rho_{\text{total}}(\text{BCP+RCP})$ (au)		
	CO <sub>2</sub>	SO <sub>2</sub>	H <sub>2</sub> S
[C <sub>1</sub> mim] <sup>+</sup>	0.017 00	0.020 35	0.010 53
[C <sub>2</sub> mim] <sup>+</sup>	0.016 94	0.019 70	0.015 17
[C <sub>3</sub> mim] <sup>+</sup>	0.016 85	0.021 71	0.015 14
[C <sub>4</sub> mim] <sup>+</sup>	0.016 86	0.021 42	0.015 22
[C <sub>5</sub> mim] <sup>+</sup>	0.016 82	0.021 53	0.015 34
[C <sub>6</sub> mim] <sup>+</sup>	0.017 15	0.021 38	0.010 33

<sup>a</sup> $\rho_{\text{total}}$  is the sum of electron density over critical points related to cation–gas interactions.

**Anion–Gas Interactions.** The results obtained from CO<sub>2</sub>-anion calculations are described in Tables 5 and 6, while data from SO<sub>2</sub>-anion and H<sub>2</sub>S-anion interactions are in Tables S2 and S3, Supporting Information.

The highest affinity with gases was exhibited by the [SO<sub>4</sub>]<sup>2-</sup>-anion, with binding energy of −353.31 kJ/mol for CO<sub>2</sub> and

occurrence of bond formation, as indicated by the negative sign of  $\nabla^2\rho$  (Table 6). Other systems that presented bond formation were F<sup>−</sup>-CO<sub>2</sub>, F<sup>−</sup>-H<sub>2</sub>S, and [SO<sub>4</sub>]<sup>2-</sup>-H<sub>2</sub>S. This fact is accompanied by elevated binding energies and electron densities over the BCPs. For example,  $\rho = 0.361800$  au for [SO<sub>4</sub>]<sup>2-</sup>-H<sub>2</sub>S (Table S3, Supporting Information) and  $\rho = 0.180742$  au for F<sup>−</sup>-CO<sub>2</sub> (Table 6). Considering not bonding systems, [Ac]<sup>−</sup> has the higher affinity with SO<sub>2</sub> and CO<sub>2</sub>, which is associated with the elevated CO<sub>2</sub> solubility in [C<sub>4</sub>mim][Ac] when compared to [C<sub>4</sub>mim][CF<sub>3</sub>COO], at low molar fractions of gas.<sup>54</sup> On the other hand, [FAP]<sup>−</sup> had the lowest affinity for the gases, with binding energy equals to −8.42 kJ/mol (Table 5) for CO<sub>2</sub>, −26.87 kJ/mol for SO<sub>2</sub>, and −17.89 kJ/mol for H<sub>2</sub>S (Table S2, Supporting Information). However, data from Zhang et al.<sup>55</sup> demonstrated that presence of fluoroalkyl chain in anion, as in the [FAP]<sup>−</sup>-anion, corresponds to higher solubility. In fact, this is a bulky anion and it presents many intermolecular interactions. Considering the fluorinated anion group, the interaction order observed is [BF<sub>4</sub>]<sup>−</sup> > [PF<sub>6</sub>]<sup>−</sup> > [Tf<sub>2</sub>N]<sup>−</sup>. Nevertheless, the experimental data indicate higher solubility of CO<sub>2</sub> in [C<sub>4</sub>mim][Tf<sub>2</sub>N] than in

**Table 4.** Electron Density ( $\rho$ ) and Laplacian of the Electron Density ( $\nabla^2\rho$ ) in the BCPs (Bond Critical Points) and RCPs (Ring Critical Points) for the Imidazolium-Based Cations Interacting with  $\text{CO}_2$ <sup>a</sup>

cation	BCP interaction	$\rho$ (au)	$\nabla^2\rho$ (au)
[C <sub>1</sub> mim] <sup>+</sup>	O19–H7	0.010183	+0.040671
	O19–H11	0.003667	+0.013336
[C <sub>2</sub> mim] <sup>+</sup>	O22–H7	0.009864	+0.039084
	O22–H13	0.003833	+0.013817
[C <sub>3</sub> mim] <sup>+</sup>	O25–H7	0.009710	+0.038345
	O25–H13	0.003881	+0.013968
[C <sub>4</sub> mim] <sup>+</sup>	O27–H7	0.009687	+0.038218
	O27–H15	0.003905	+0.014048
[C <sub>5</sub> mim] <sup>+</sup>	O31–H7	0.009661	+0.038093
	O31–H15	0.003898	+0.014026
[C <sub>6</sub> mim] <sup>+</sup>	O32–O13	0.009539	+0.037414
	O32–H17	0.004224	+0.014966
cation	RCP-6 atoms $\rho$ (au)	$\nabla^2\rho$ (au)	
[C <sub>1</sub> mim] <sup>+</sup>	0.003191	+0.013538	
[C <sub>2</sub> mim] <sup>+</sup>	0.003245	+0.013786	
[C <sub>3</sub> mim] <sup>+</sup>	0.003258	+0.013851	
[C <sub>4</sub> mim] <sup>+</sup>	0.003268	+0.013893	
[C <sub>5</sub> mim] <sup>+</sup>	0.003263	+0.013874	
[C <sub>6</sub> mim] <sup>+</sup>	0.003384	+0.014411	

<sup>a</sup>All O atoms are related to the  $\text{CO}_2$  molecule, while all H atoms are from the cation imidazolium.

[C<sub>4</sub>mim][PF<sub>6</sub>]<sup>15,56</sup> The topological graphics for the lowest energy structure related to [Tf<sub>2</sub>N]<sup>+</sup>–CO<sub>2</sub> interaction are given in Figure 6. There, three sites of interaction can be evidenced, where the anion interaction sites are O7, O8, and F12, with the following values for the electron density, 0.007592, 0.007570, and 0.001388 au. That higher electron density at BCP for the oxygen sites is a strong indication that the interaction strength is mainly due to the oxygen atom, corroborating to the interaction energy calculations such as described recently in the literature.<sup>35,57</sup> The topological graphics for other anion–gas interactions are shown in the Supporting Information (Figure S2).

As mentioned previously, the [SO<sub>4</sub>]<sup>2−</sup> anion presented bond formation with the CO<sub>2</sub> molecule, which is evidenced by Figure 7A, which describes the charge distribution of [SO<sub>4</sub>]<sup>2−</sup>–CO<sub>2</sub>. We can note the negative charge concentrated in the oxygen that interacts with gas. Nevertheless, the addition of the alkyl chain in the sulfate group promotes a better charge distribution over the ion (Figure 7B). Then, the interaction site becomes less negative and weaker. The binding energy for the [SO<sub>4</sub>]<sup>2−</sup>–CO<sub>2</sub> system is −353.31 kJ/mol, while for [MeSO<sub>4</sub>]<sup>−</sup>–CO<sub>2</sub> it is −22.29 kJ/mol. On the other hand, the alkyl chain variation for [EtSO<sub>4</sub>]<sup>−</sup> and [BuSO<sub>4</sub>]<sup>−</sup> does not modify significantly the binding energies.

The analysis of solubility data shows that CO<sub>2</sub> has lower solubility than H<sub>2</sub>S in [MeSO<sub>4</sub>]<sup>−</sup> systems, whose binding energy is −39.94 kJ/mol (Table S2, Supporting Information).<sup>27</sup> It is due to the occurrence of H-bonds in [MeSO<sub>4</sub>]<sup>−</sup>–H<sub>2</sub>S systems (Table S3, Supporting Information), with  $\rho = 0.029140$  au and  $\nabla^2\rho = +0.094839$  au. Then, [MeSO<sub>4</sub>]<sup>−</sup> is an alkylsulfate capable of separating efficiently H<sub>2</sub>S from CO<sub>2</sub>. [Tf<sub>2</sub>N]<sup>+</sup> also exhibits H-bonds with H<sub>2</sub>S, whose interactions are stronger than [Tf<sub>2</sub>N]<sup>+</sup>–CO<sub>2</sub> ones. According to Jalili et al.,<sup>8</sup> H-bonds in [Tf<sub>2</sub>N]<sup>+</sup>–H<sub>2</sub>S are responsible for the higher H<sub>2</sub>S solubility in [C<sub>4</sub>mim][Tf<sub>2</sub>N] than CO<sub>2</sub> in the same IL. Other systems that exhibit H-bonds between anion–H<sub>2</sub>S include [EtSO<sub>4</sub>]<sup>−</sup> and [BuSO<sub>4</sub>]<sup>−</sup>, whose AIM data are given in Table S3 in the Supporting Information.

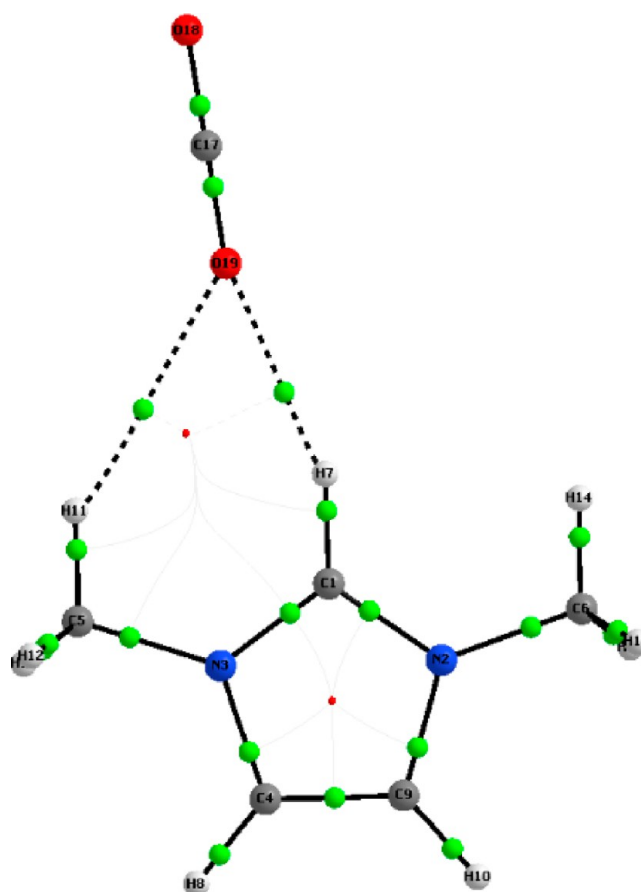


**Figure 2.** Topological graphic of [C<sub>1</sub>mim]<sup>+</sup>–CO<sub>2</sub> obtained from AIM analysis. The dashed black lines correspond to weak interactions and the solid black ones to covalent bonds. In evidence is the interaction between the oxygen from CO<sub>2</sub> (O19) and the two hydrogen atoms from cation (H11 and H7). The gray, red, blue, and white spheres represent carbon, oxygen, nitrogen, and hydrogen atoms, respectively. The green balls indicate Bond Critical Points (BCPs) and the tiny red one, the Ring Critical Point (RCP).

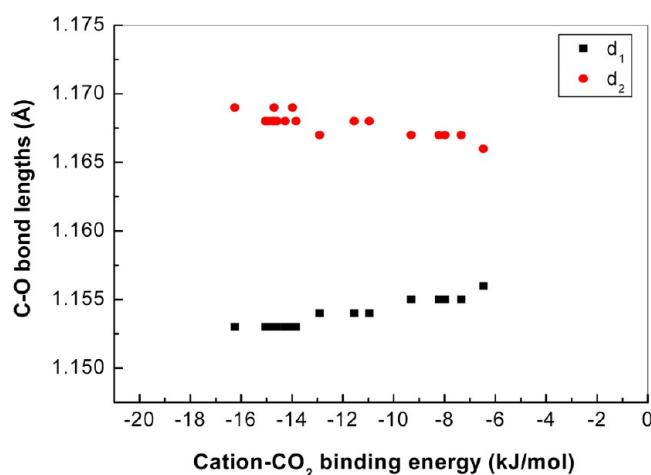


**Figure 3.** Relation between the CO<sub>2</sub> bond lengths and the cation–CO<sub>2</sub> binding energies (kJ/mol). The red circles and black squares correspond to  $d_2$  (C–O involved in the interaction with gas) and  $d_1$  (not involved in it), respectively.

In contrast to what occurs with the cations, anion–gas interactions (mainly CO<sub>2</sub> and SO<sub>2</sub> gases) promote a little changing in the C–O and S–O bond length symmetrically. As an example,

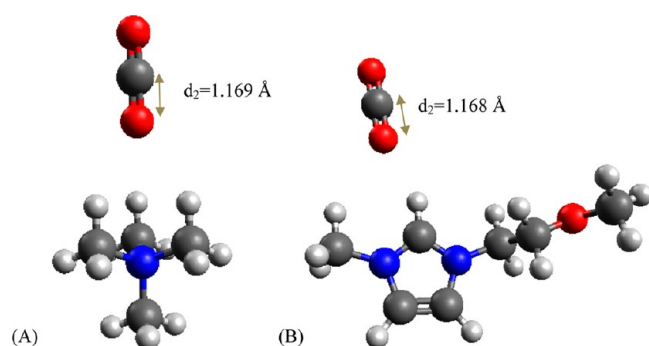


**Figure 4.** Schematic representation for  $[\text{TMA}]^+\cdot\text{CO}_2$  (A) and  $[\text{C}_1\text{Oemim}]^+\cdot\text{CO}_2$  (B) optimized geometries, at the B3LYP/6-311+G\*\* level of theory, highlighting the distance of the C–O bond near the cation interaction site. The gray, red, and blue spheres correspond to carbon, oxygen, and nitrogen atoms, respectively.

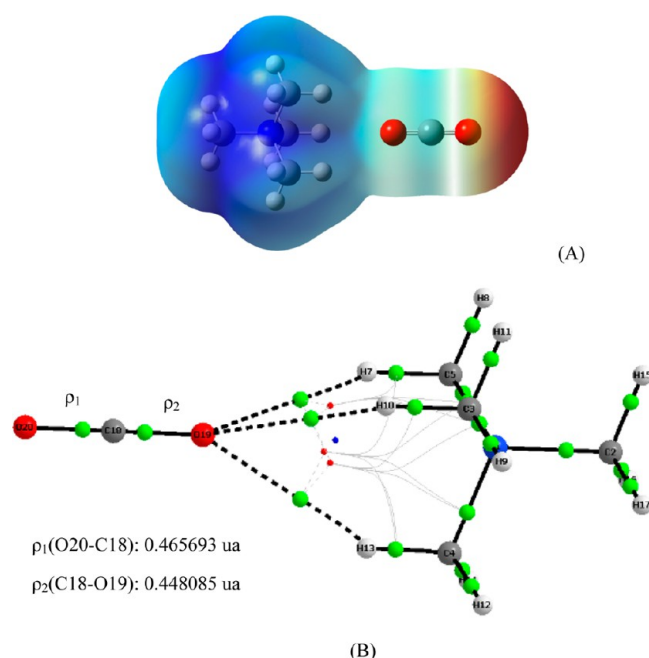


**Figure 5.** Schematic representation of the electrostatic potential map (A) and the topological graphics of the critical points (B) for the  $[\text{TMA}]^+\cdot\text{CO}_2$  system. The medium gray, blue, red, and white spheres represent the carbon, nitrogen, oxygen, and hydrogen atoms, respectively. Isovalue: 0.0004; scale:  $-0.070$ – $0.160$  at the B3LYP/6-311+G\*\* level of theory.

the C–O bond length for iodide- $\text{CO}_2$  is  $1.174 \text{ \AA}$  (C–O from isolated gas is  $1.161 \text{ \AA}$ ), while for bromide it is  $1.164 \text{ \AA}$ . For  $\text{H}_2\text{S}$ , there is an unequal change of the two intermolecular distances and the bond length suffers a deviation proportional to the binding energy. However, due to the Lewis acid–base interaction,<sup>8</sup> there is an electron repulsion between oxygen atoms from  $\text{CO}_2$  (and  $\text{SO}_2$ ) and the anion. So, the angle of the gas deviates from the isolated state ( $180^\circ$  for  $\text{CO}_2$  and  $118^\circ$  for  $\text{SO}_2$ ). Figure 8 shows a remarkable linear relation between binding energy and OSO angle, with distortion changed from  $3.4^\circ$   $[\text{FAP}]^-$  to  $8.6^\circ$   $[\text{SO}_4]^{2-}$ . Such relation is also valid for anion- $\text{CO}_2$  interactions (see Figure S3 in the Supporting Information) and is in good agreement with the literature.<sup>14</sup>

**Vibrational Frequencies and Split.** All systems studied in this work presented positive values for vibrational frequencies, and consequently, correspond to minimum states. According to

**Table 5.** Data Obtained from Anion–Gas Calculations<sup>a</sup>

anion/gas	$\text{CO}_2$			
	$E_0+\text{ZPE}$ (hartrees)	$\Delta E_{\text{CP}}$ (kJ/mol)	$\text{CO}_2$ angle (deg)	$d_{\text{min}}$ (Å)
$\text{F}^-$	−288.5730	−271.64	138.2	1.521
$\text{Cl}^-$	−648.9487	−35.43	167.9	2.916
$\text{Br}^-$	−2762.8802	−24.95	171.2	3.230
$\text{I}^*$	−7108.5710	−17.21	173.3	3.612
$[\text{TF}_2\text{N}]^-$	−2016.2000	−15.79	175.8	2.911
$[\text{TFA}]^-$	−1150.3457	−19.68	174.6	2.777
$[\text{BF}_4]^-$	−613.3085	−21.55	174.5	2.825
$[\text{PF}_6]^-$	−1129.5188	−14.87	175.8	2.910
$[\text{FAP}]^-$	−2556.5041	−8.42	177.0	2.819
$[\text{Ac}]^-$	−417.2033	−57.23	163.5	2.328
$[\text{SO}_4]^{2-}$	−887.7790	−353.31	132.8	1.491
$[\text{MeSO}_4]^-$	−927.7343	−22.27	173.5	2.626
$[\text{EtSO}_4]^-$	−967.0360	−23.29	174.4	2.672
$[\text{BuSO}_4]^-$	−1045.6291	−22.79	173.7	2.715

<sup>a</sup>The columns describe electronic energy with ZPE correction ( $E_0+\text{ZPE}$ ), binding energies with BSSE correction ( $\Delta E_{\text{CP}}$ ), and gas angle after interaction and minimum distance ( $d_{\text{min}}$ ), at the B3LYP/6-311+G\*\* level of theory, but  $\text{I}^-$  (DGDVZP)\*.

**Table 6.** Data Obtained from AIM Analysis over BCPs for the Anion– $\text{CO}_2$  Systems<sup>a</sup>

anion	$\text{CO}_2$			
	BCP	$\rho$ (au)	$\nabla^2\rho$ (au)	$\rho_{\text{total}}$ (au)
$\text{F}^-$	C2–F1	0.180742	−0.068955	0.180742
$\text{Cl}^-$	C2–Cl1	0.015950	+0.043990	0.015950
$\text{Br}^-$	C2–Br1	0.010704	+0.029610	0.010704
$\text{I}^-$	C2–I1	0.007342	+0.018551	0.007342
$[\text{TFA}]^-$	O2–C9	0.011549	+0.043570	0.011549
$[\text{FAP}]^-$	C26–F3	0.008011	+0.038439	0.011167
	O27–F24	0.001614	+0.009142	
$[\text{PF}_6]^-$	C8–F3	0.007146	+0.033485	0.019647
	C8–F6	0.007142	+0.033466	
$[\text{BF}_4]^-$	C6–F3	0.008864	+0.038281	0.024208
	C6–F4	0.008774	+0.037974	
$[\text{TF}_2\text{N}]^-$	C16–O7	0.007592	+0.033351	0.022012
	C16–O8	0.007570	+0.033361	
	O17–F12	0.001388	+0.007974	
$[\text{Ac}]^-$	O3–C8	0.032560	+0.088676	0.032560
$[\text{SO}_4]^{2-}$	C6–O2	0.215940	−0.338126	0.215940
$[\text{MeSO}_4]^-$	O2–C12	0.014821	+0.057678	0.014821
$[\text{EtSO}_4]^-$	O3–C13	0.014141	+0.053187	0.014141
$[\text{BuSO}_4]^-$	O3–C19	0.013337	+0.048638	0.013337
anion	RCP atoms	$\rho$ (au)	$\nabla^2\rho$ (au)	
$[\text{BF}_4]^-$	4	0.006570	+0.034532	
$[\text{PF}_6]^-$	4	0.005359	+0.029120	
$[\text{TF}_2\text{N}]^-$	6	0.004098	+0.021155	
	6	0.001364	+0.007855	
$[\text{FAP}]^-$	4	0.001542	+0.009622	

<sup>a</sup> $\rho$  describes the electron density and ( $\nabla^2\rho$ ) the Laplacian of the density.  $\rho_{\text{total}}$  is the sum of the electronic density for all BCPs and RCPs.

Shimanouchi,<sup>58</sup> the  $\text{CO}_2$  bending frequency in the gaseous phase is  $670.09 \text{ cm}^{-1}$ , which was measured with  $\text{N}_2$  in Dow KBr Foreprism Equipment. The calculated values with the B3LYP/6-311G\*\* level of theory were  $668.5$  and  $642.7 \text{ cm}^{-1}$ , without and with correction, respectively. For isolated gas, in-plane and out-of-plane bending modes are identical, while symmetric and



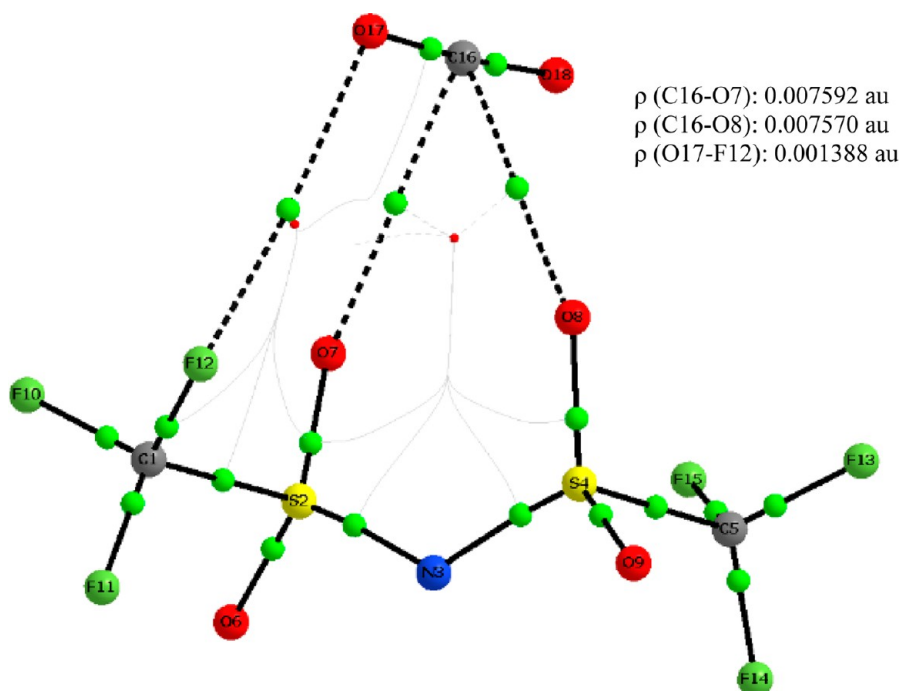


**Figure 6.** Topological graphics of the critical points for the  $[\text{Tf}_2\text{N}]^- \text{CO}_2$  interactions at the B3LYP/6-311+G\*\* level of theory. The medium gray, blue, red, white, green, and yellow spheres represent the carbon, nitrogen, oxygen, hydrogen, fluorine, and sulfur atoms, respectively.

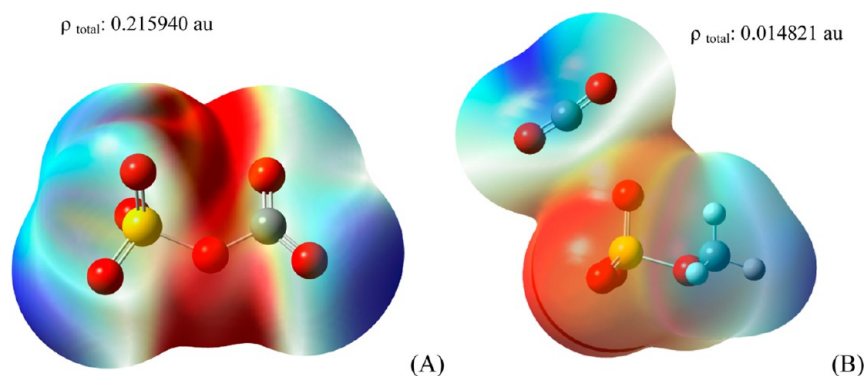


**Figure 7.** Schematic representation of the electrostatic potential map for  $[\text{sulfate}]^- \text{CO}_2$  (A) isovalue 0.0004, scale  $-0.350$ – $0.350$ , and  $[\text{MeSO}_4]^- \text{CO}_2$  (B) isovalue 0.004, scale  $-0.180$ – $0.080$ .

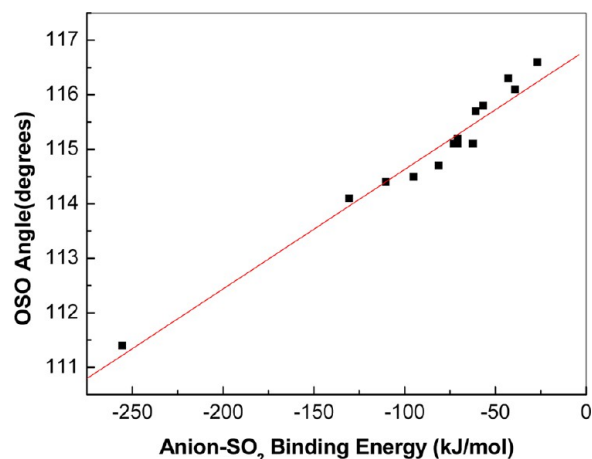


**Figure 8.** Relation between  $\text{SO}_2$  angle and anion- $\text{SO}_2$  binding energies.  $R = 0.97731$ .

asymmetric stretching modes having frequencies of  $1373.0$  and  $2420.0 \text{ cm}^{-1}$ , respectively.

The symmetric stretching frequencies ranged from  $1284.6 \text{ cm}^{-1}$ , for  $[\text{SO}_4]^{2-} \text{CO}_2$ , to  $1373.5 \text{ cm}^{-1}$ , for  $[\text{TBA}]^+ \text{CO}_2$ , with small variation for cations ( $\Delta\nu \leq 5 \text{ cm}^{-1}$ ) and anions from the same group, as alkylsulfate ( $\Delta\nu \leq 0.5 \text{ cm}^{-1}$ ). The asymmetric stretching mode of  $\text{CO}_2$  ranges from  $1764.0 \text{ cm}^{-1}$  for sulfate- $\text{CO}_2$  ( $\Delta\nu = 656.0 \text{ cm}^{-1}$ ) and  $2424.9 \text{ cm}^{-1}$  for  $[\text{C}_1\text{mim}]^+ \text{CO}_2$  ( $\Delta\nu = 4.9 \text{ cm}^{-1}$ ).  $\Delta\nu$  is the difference between the normal-mode frequency for the interacting gas and the isolated one.

As is well-known, the bending mode is doubly degenerated for gaseous  $\text{CO}_2$ . Therefore, a doublet caused by deviation from linear geometry is observed.<sup>14</sup> Data containing in-plane ( $\nu_{2a}$ ) and out-of-plane ( $\nu_{2b}$ ) bending modes, in  $\text{cm}^{-1}$ , are given in Table S5 (Supporting Information). In the last column are the data of deviation between these two modes ( $\Delta\nu'$ ), also called frequency split, which is directly related to strength interaction and, consequently, with the deviation from linearity. Figure 9 presents the dependence of the  $\text{CO}_2$  bending angle deviation with frequency split for all anion- $\text{CO}_2$  interactions. For the cation- $\text{CO}_2$  interactions, due to little variation of the gas angle,  $\Delta\nu'$  is  $1$ – $2 \text{ cm}^{-1}$ .



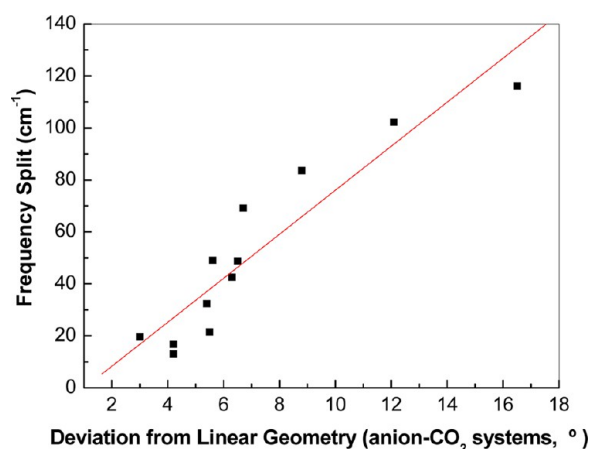


**Figure 9.** Relation between frequency split ( $\Delta\nu'$ ) and  $\text{CO}_2$  angle deviation for anion–gas interactions in comparison with the isolated gas ( $180.0^\circ$ ).  $R = 0.93022$ .

and it is not possible to evaluate its relation with interaction strength.

The sulfur dioxide ( $\text{SO}_2$ ) and hydrogen sulfide ( $\text{H}_2\text{S}$ ) are nonlinear molecules with three vibrational modes: bending ( $\nu_2$ ), symmetric ( $\nu_1$ ), and asymmetric ( $\nu_3$ ). The experimental frequencies for  $\nu_1$  and  $\nu_3$  modes ( $\text{SO}_2$ ) appear between 1000 and 1500  $\text{cm}^{-1}$ , and for  $\text{H}_2\text{S}$  are equal to 2614.6 and 2626.0  $\text{cm}^{-1}$ , while  $\nu_2$  appears at 19  $\text{cm}^{-1}$  ( $\text{SO}_2$ ) and 1182.7  $\text{cm}^{-1}$  ( $\text{H}_2\text{S}$ ).<sup>58,59</sup> The calculated values for  $\text{SO}_2$  are 1131.0  $\text{cm}^{-1}$  ( $\nu_1$ ), 1309.7  $\text{cm}^{-1}$  ( $\nu_3$ ), and 504.0  $\text{cm}^{-1}$  for the  $\nu_2$  bending mode. Due to the low interaction strength for the cation, angle deviations are not significant. For the anions, the lowest deviation compared to isolated gas for symmetric and asymmetric modes was exhibited by  $[\text{FAP}]^-\text{-SO}_2$ , with 1127.3 and 1284.1  $\text{cm}^{-1}$ , while the highest were shown by  $[\text{SO}_4]^{2-}\text{-SO}_2$ , with 1040.0 and 1106.0  $\text{cm}^{-1}$ . The bending mode varies from 451.4  $\text{cm}^{-1}$  ( $[\text{sulfate}]^-\text{-SO}_2$ ) to 519.0  $\text{cm}^{-1}$  ( $[\text{Ac}]^-\text{-SO}_2$ ). Considering the halide group, there is less variation in frequency with increasing of the ionic radius. For  $\text{H}_2\text{S}$ , the calculated values for symmetric and asymmetric modes were respectively 2679.4, 2694.8, and 1208.0  $\text{cm}^{-1}$ , for the bending mode. Figure S4 (Supporting Information) exhibits the linear relation between the symmetric stretching mode and the H–S bond length after interaction. In fact, the anion– $\text{H}_2\text{S}$  interaction strength is related to the H–S bond stretching, changing the vibration frequency compared to the isolated gas.

**Comparison between the Gases.** Figures 10 and 11 summarize the binding energies for the cation–gas and anion–gas interactions, respectively.

We can note that the stronger interactions occur for  $\text{SO}_2$ , where the affinity with both cation and anion can be established as  $\text{SO}_2 > \text{H}_2\text{S} > \text{CO}_2$ . Considering interactions between gases and ILs are Lewis acid–base type,<sup>2,29</sup> these systems can be grouped in an empirical classification as hard and soft. Such concepts are related to the atom polarizability, where soft acids and bases are highly polarizable, while hard ones are not.<sup>61</sup> The hardness and softness order of the molecules or ions were calculated through eq 1 and are expressed in Table S6, Supporting Information.<sup>60,61</sup>

$$\eta = \frac{E_{\text{LUMO}} - E_{\text{HOMO}}}{2} \sigma = 1/\eta \quad (1)$$

The lowest HOMO–LUMO gap was found for  $\text{SO}_2$  (2.678 eV). Therefore, this gas is softer and more polarizable, in other words, there is higher ability to disperse the electron cloud, favoring the

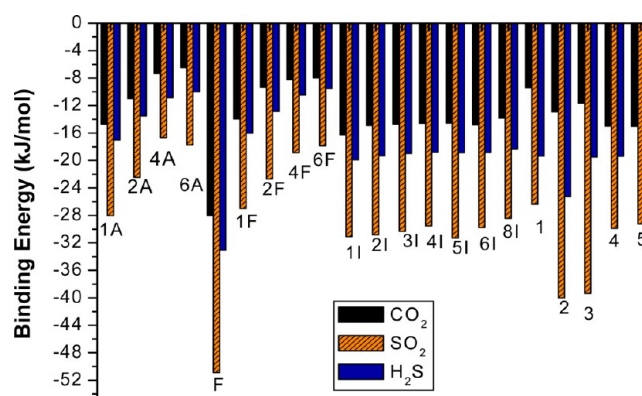


**Figure 10.** Binding energies (kJ/mol) for cation–gas interactions:  $[\text{TMA}]^+\text{-1A}$ ;  $[\text{TEA}]^+\text{-2A}$ ;  $[\text{TBA}]^+\text{-4A}$ ;  $[\text{THA}]^+\text{-6A}$ ;  $[\text{Phosphonium}]^+\text{-F}$ ; 1F, 2F, 4F, 6F, correspond to  $[\text{TMF}]^+$ ,  $[\text{TEF}]^+$ ,  $[\text{TBF}]^+$ ,  $[\text{THF}]^+$ ; 1I– $[\text{C}_1\text{mim}]^+$ ; 2I– $[\text{C}_2\text{mim}]^+$ ; 3I– $[\text{C}_3\text{mim}]^+$ ; 4I– $[\text{C}_4\text{mim}]^+$ ; 5I– $[\text{C}_5\text{mim}]^+$ ; 6I– $[\text{C}_6\text{mim}]^+$ ; 8I– $[\text{C}_8\text{mim}]^+$ ; 1– $[\text{C}_1\text{Odmim}]^+$ ; 2– $[\text{C}_1\text{OC}_3\text{Odmim}]^+$ ; 3– $[\text{C}_1\text{OC}_2\text{Odmim}]^+$ ; 4– $[\text{C}_1\text{OC}_2\text{Oemim}]^+$ ; 5– $[\text{C}_1\text{Oemim}]^+$  at the B3LYP/6-311+G\*\* level of theory.

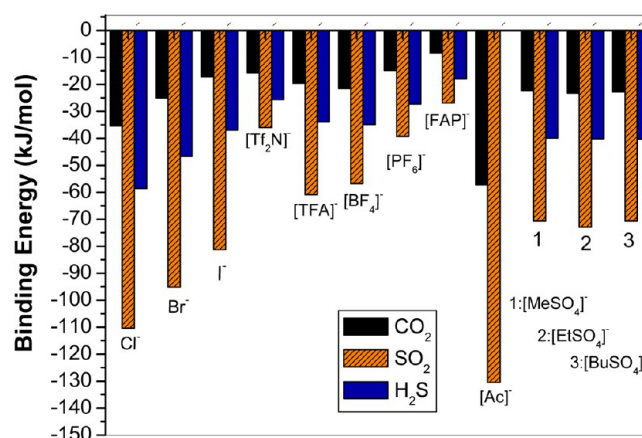


**Figure 11.** Binding energy (kJ/mol) for anion–gas interactions.  $[\text{SO}_4]^{2-}$  and  $\text{F}^-$  are not represented due to the high values associated with the bond formation.

**Table 7. Data Obtained from Electronic Structure Calculations for  $[\text{C}_1\text{mim}]^+\text{-Anion Systems}$  at the B3LYP Level of Theory, 6-311+G\*\* Basis Set<sup>a</sup>**

system	$E_0 + \text{ZPE}$ (hartrees)	$\Delta E_{\text{AB}}$ (kJ/mol) B3LYP	$\Delta E_{\text{CP}}$ (kJ/mol) B3LYP	$d_{\text{min}}$ (Å) B3LYP
$[\text{C}_1\text{mim}]$ $[\text{Tf}_2\text{N}]$	−2132.847 95	−337.81	−327.21	2.012
$[\text{C}_1\text{mim}]$ $[\text{BF}_4]$	−729.966 79	−353.57	−357.05	2.060
$[\text{C}_1\text{mim}]$ $[\text{MeSO}_4]$	−1044.396 60	−363.68	−368.11	1.941
$[\text{C}_1\text{mim}]$ $[\text{EtSO}_4]$	−1083.698 15	−363.58	−368.56	1.960
$[\text{C}_1\text{mim}]$ $[\text{BuSO}_4]$	−1162.290 18	−361.62	−366.72	1.988
$[\text{C}_1\text{mim}]$ $[\text{PF}_6]$	−1246.169 64	−328.16	−332.70	2.140

<sup>a</sup>Electronic energy with zero point correction ( $E_0 + \text{ZPE}$ ), binding energy without BSSE correction ( $\Delta E_{\text{AB}}$ ) and with BSSE correction ( $\Delta E_{\text{CP}}$ ), and the minimum distance of interaction ( $d_{\text{min}}$ ).

interaction with ion. In sequence are  $\text{H}_2\text{S}$  and  $\text{CO}_2$ , with 3.513 and 4.982 eV, respectively, a tendency that is in good agreement

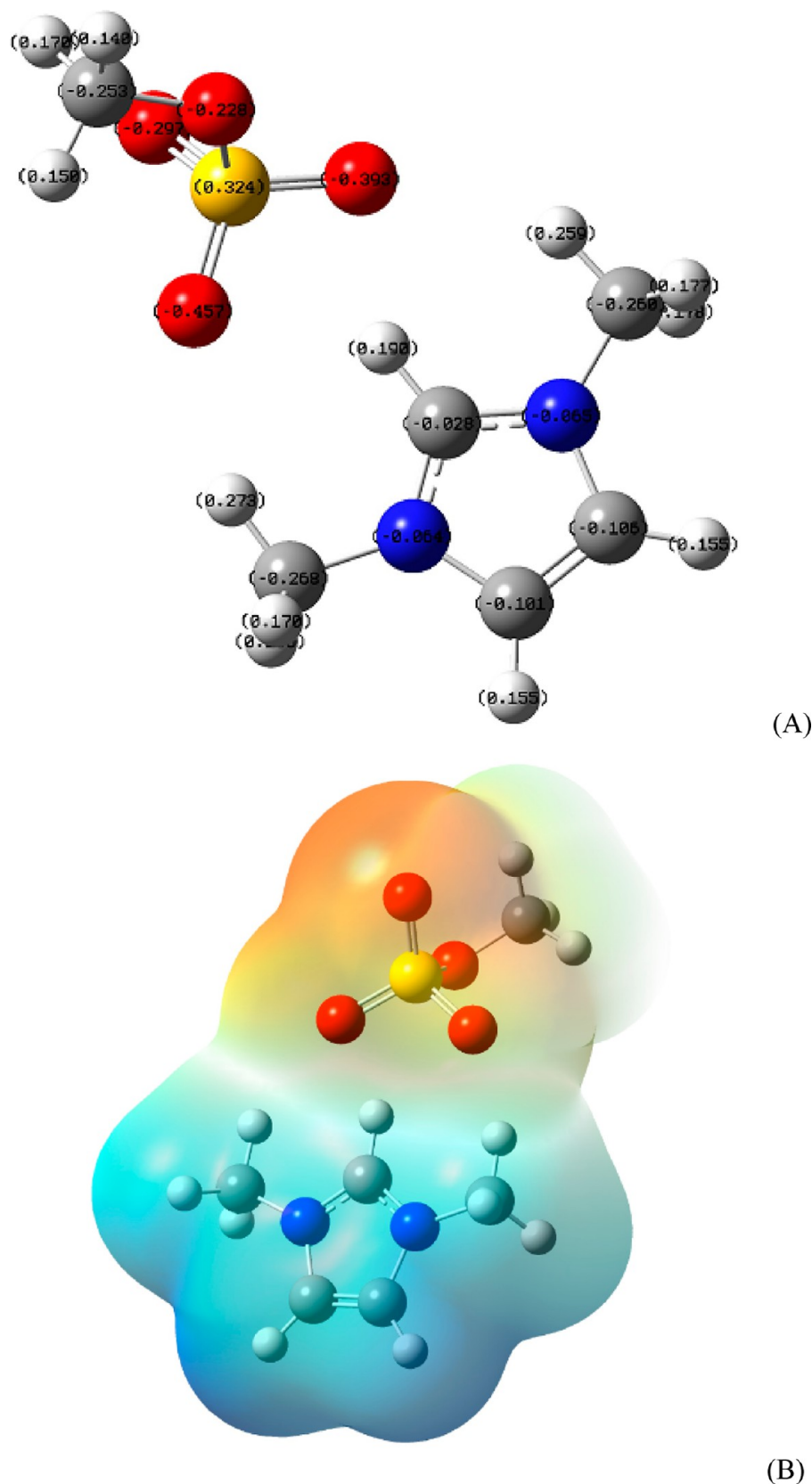


**Figure 12.** Schematic representation of partial charges (A) and electrostatic potential map (B) for  $[\text{C}_1\text{mim}][\text{MeSO}_4]$ . The medium gray, blue, red, white, and yellow spheres represent the carbon, nitrogen, oxygen, hydrogen, and sulfur atoms, respectively. Scale:  $-0.010$ – $0.080$ ; isovalue:  $0.0004$ .

with polarizability data from the literature.<sup>62</sup> The high polarizability presented by  $\text{H}_2\text{S}$  compared to  $\text{CO}_2$  has been associated with the higher solubility of  $\text{H}_2\text{S}$  in  $[\text{C}_n\text{mim}][\text{Tf}_2\text{N}]$ , according to

Jalili et al.<sup>8</sup> The direct correlation between gas polarizability and its solubility in IL is also described by Brennecke et al.<sup>64</sup> This occurs due to the domain of the dispersive interaction forces

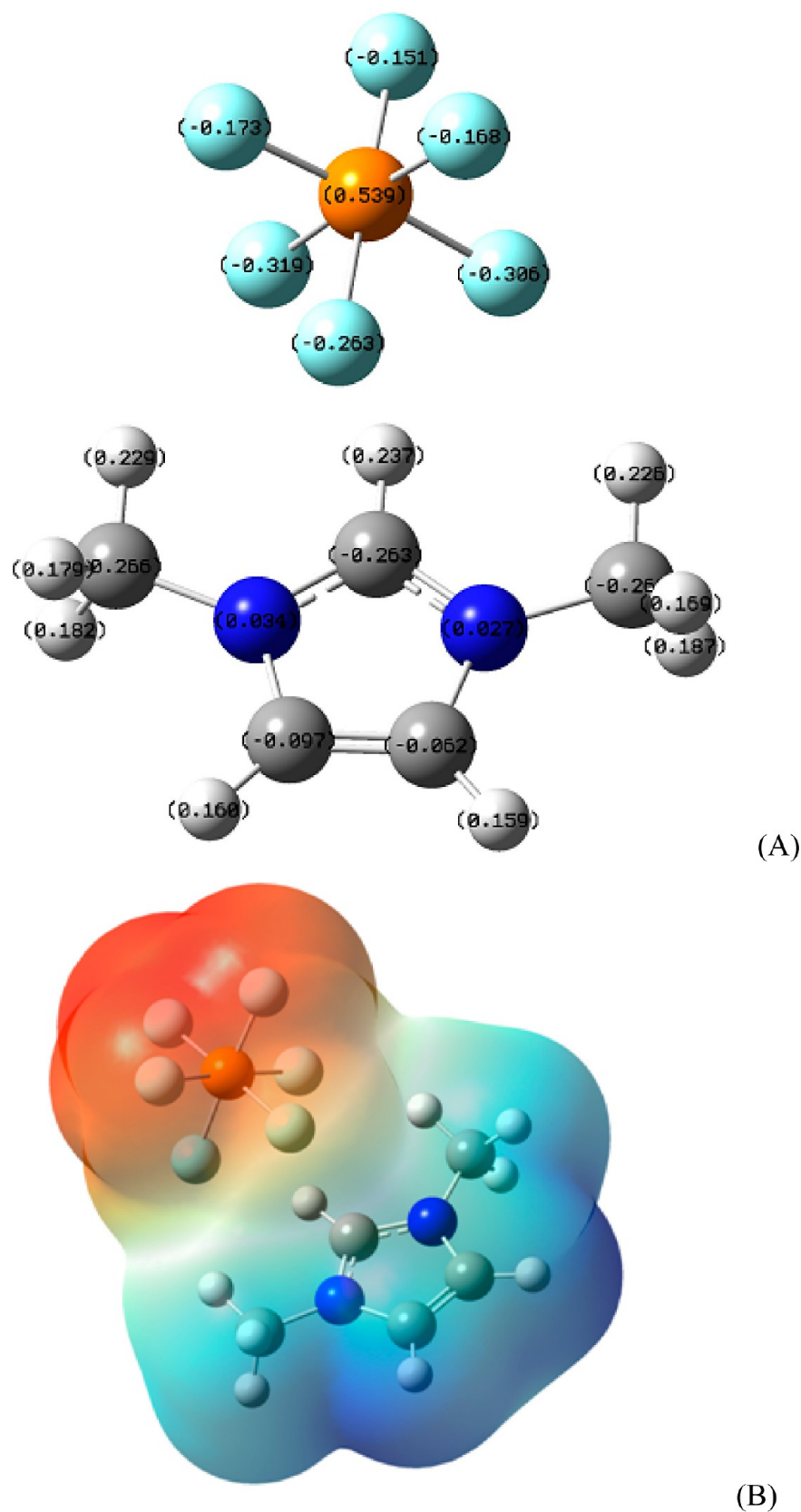


**Figure 13.** Partial charges (A) and electrostatic potential map (B) for [C<sub>1</sub>mim][PF<sub>6</sub>]. The medium gray, dark blue, white, light blue, and orange spheres represent the carbon, nitrogen, hydrogen, fluorine, and phosphorus atoms, respectively. Scale:  $-0.075$  to  $0.070$ ; isovalue:  $0.0004$ .

between gas and IL. However, among the series studied by the authors, CO<sub>2</sub> has relatively high solubility due to the presence of quadrupole moment and specific interactions between gas and

anion.<sup>63,64</sup> So, we can say that polarizability and, consequently, the binding energy are not the only factors that determine the gas solubility in ionic liquids.

**Table 8.** Data Obtained from Electronic Structure Calculations for Imidazolium-Based Systems at the B3LYP and M06-2X/6-311+G\*\* Levels of Theory<sup>a</sup>

ionic pair	$E_0 + \text{ZPE}$ (hartrees)	$\Delta E_{\text{AB}}$ (kJ/mol)	$\Delta E_{\text{CP}}$ (kJ/mol)	$d_{\text{min}}$ (Å)	level of theory
[C <sub>1</sub> mim][Tf <sub>2</sub> N]	−2132.847952	−337.81	−327.21	2.012	B3LYP
		−364.79	−365.40	2.104	M06-2X
[C <sub>2</sub> mim][Tf <sub>2</sub> N]	−2172.146 60	−331.73	−321.14	1.991	B3LYP
		−358.36	−360.87	2.413	M06-2X
[C <sub>3</sub> mim][Tf <sub>2</sub> N]	−2211.442 65	−331.03	−318.49	2.005	B3LYP
		−364.59	−363.18	2.128	M06-2X
[C <sub>4</sub> mim][Tf <sub>2</sub> N]	−2250.739 20	−330.95	−317.77	2.002	B3LYP
		−367.41	−365.85	2.272	M06-2X
[C <sub>6</sub> mim][Tf <sub>2</sub> N]	−2329.332 42	−329.29	−317.81	1.929	B3LYP
		−358.11	−360.27	2.071	M06-2X
[C <sub>8</sub> mim][Tf <sub>2</sub> N]	−2407.923 07	−333.65	−313.41	2.223	B3LYP
		−349.72	−351.89	2.071	M06-2X

<sup>a</sup>The columns describe electronic energy with ZPE correction ( $E_0 + \text{ZPE}$ ), binding energies without and with BSSE correction ( $\Delta E_{\text{AB}}$  and  $\Delta E_{\text{CP}}$ ), gas angle after interaction, and minimum distance of interaction ( $d_{\text{min}}$ ).

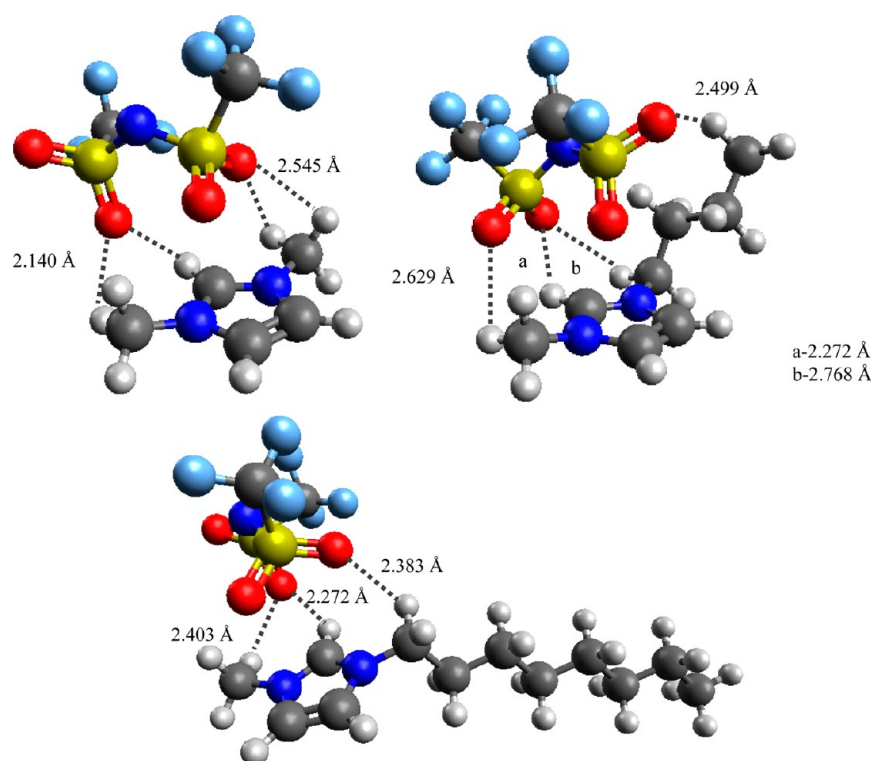


**Figure 14.** Optimized geometries of the [C<sub>1</sub>mim][Tf<sub>2</sub>N] (A), [C<sub>4</sub>mim][Tf<sub>2</sub>N] (B), and [C<sub>8</sub>mim][Tf<sub>2</sub>N] (C) ion pairs at the M06-2X/6-311+G\*\* level of theory. The gray, red, dark blue, light blue, yellow, and white spheres represent carbon, oxygen, nitrogen, fluorine, sulfur, and hydrogen atoms, respectively. In evidence, some interaction distances.

**Ion Pairs Contribution.** Results from electronic calculations for [C<sub>1</sub>mim]<sup>+</sup>-based systems and variable anion are described in Table 7, at the B3LYP/6-311+G\*\* level. The range comprises −327.21 kJ/mol ([C<sub>1</sub>mim][Tf<sub>2</sub>N]) to −368.56 kJ/mol, for ([C<sub>1</sub>mim][EtSO<sub>4</sub>]). The minimum distances are generally proportional to the strength interaction, with 2.012 and 1.960 Å, respectively. Comparing with cation–gas and anion–gas calculations, the binding energy for ion pairs is higher in magnitude. For example, [phosphonium]<sup>+</sup>–CO<sub>2</sub> has  $\Delta E_{\text{CP}} = -28.05$  kJ/mol and [Ac]<sup>−</sup>–CO<sub>2</sub> has  $\Delta E_{\text{CP}} = -57.23$  kJ/mol, considering not bonding systems. The magnitude order of the binding energy is [C<sub>1</sub>mim][EtSO<sub>4</sub>]  $\approx$  [C<sub>1</sub>mim][MeSO<sub>4</sub>] > [C<sub>1</sub>mim][BuSO<sub>4</sub>] > [C<sub>1</sub>mim][BF<sub>4</sub>] > [C<sub>1</sub>mim][PF<sub>6</sub>] > [C<sub>1</sub>mim][Tf<sub>2</sub>N]. This difference occurs due to the lower charge distribution presented by [C<sub>1</sub>mim][MeSO<sub>4</sub>]

and [C<sub>1</sub>mim][EtSO<sub>4</sub>] compared to other ion pairs. The charge distributions of [C<sub>1</sub>mim][PF<sub>6</sub>] and [C<sub>1</sub>mim][MeSO<sub>4</sub>] are explained in Figures 12 and 13, respectively.

In spite of the fact that the two anions present the same oxidation number (−1), [PF<sub>6</sub>]<sup>−</sup> has charge distributed in higher volume compared to [MeSO<sub>4</sub>]<sup>−</sup>. The partial charges indicate that fluorine atoms ([PF<sub>6</sub>]<sup>−</sup>) are less electronegative than oxygen atoms from [MeSO<sub>4</sub>]<sup>−</sup> (maximum charge partial of −0.319e for [PF<sub>6</sub>]<sup>−</sup> and −0.457e for [MeSO<sub>4</sub>]<sup>−</sup>), resulting from the higher charge density in the C<sub>1</sub>mim⋯MeSO<sub>4</sub> interaction, corroborating the binding energy results. In this sense, the hydrogen atoms involved in the interaction with anion also exhibit variations in the partial charges (Figures 12A and 13A). The hydrogen bonded with C=N has partial charge of 0.190e in [C<sub>1</sub>mim][MeSO<sub>4</sub>] and



**Table 9.** Data Obtained from Electronic Structure Calculations for Ether-Functionalized Imidazolium Based Systems at the B3LYP and M06-2X/6-311+G\*\* Levels of Theory<sup>a</sup>

system	$E_0 + \text{ZPE}$	$\Delta E_{\text{AB}}$ (kJ/mol)	$\Delta E_{\text{CP}}$ (kJ/mol)	$d_{\text{min}}$ (Å)	level of theory
[C <sub>1</sub> Odmim][Tf <sub>2</sub> N]	−2247.368 15	−342.39	−331.44	2.037	B3LYP
		−376.19	−376.31	2.135	M06-2X
[C <sub>1</sub> OC <sub>3</sub> Odmim][Tf <sub>2</sub> N]	−2440.481 73	−333.75	−329.07	2.049	B3LYP
		−379.90	−376.86	2.233	M06-2X
[C <sub>1</sub> OC <sub>2</sub> Odmim][Tf <sub>2</sub> N]	−2401.182 65	−336.44	−325.60	2.005	B3LYP
		−368.46	−386.50	2.412	M06-2X
[C <sub>1</sub> OC <sub>2</sub> Oemim][Tf <sub>2</sub> N]	−2440.474 98	−333.44	−326.07	1.989	B3LYP
		−369.75	−380.32	2.310	M06-2X
[C <sub>1</sub> Oemim][Tf <sub>2</sub> N]	−2286.660 99	−333.19	−323.77	1.953	B3LYP
		−365.90	−364.11	2.393	M06-2X

<sup>a</sup>The columns describe electronic energy with ZPE correction ( $E_0 + \text{ZPE}$ ), binding energies without and with BSSE correction ( $\Delta E_{\text{AB}}$  and  $\Delta E_{\text{CP}}$ ), and gas angle after interaction and minimum distance of interaction ( $d_{\text{min}}$ ).

0.237 $e$  in [C<sub>1</sub>mim][PF<sub>6</sub>]. However, the hydrogen atoms from the methyl group present partial charge of 0.273 $e$  and 0.259 $e$  in [C<sub>1</sub>mim][MeSO<sub>4</sub>], and 0.229 $e$  and 0.226 $e$  in [C<sub>1</sub>mim][PF<sub>6</sub>]. It is possible to note that the charge centers P and S have decreased charge from 0.600 $e$  and 0.500 $e$  (isolated) to 0.539 $e$  and 0.324 $e$  (after interaction), respectively, which is a result from the charge transfer and, consequently, from its charge redistribution.

As was described previously, the anion–gas affinity is steeper than that observed for cation–gas ([C<sub>4</sub>mim]<sup>+</sup>·CO<sub>2</sub> = −14.62; [C<sub>4</sub>mim]<sup>+</sup>·H<sub>2</sub>S = −18.82; [Tf<sub>2</sub>N]<sup>−</sup>·CO<sub>2</sub> = −15.79; [PF<sub>6</sub>]<sup>−</sup>·CO<sub>2</sub> = −14.87; [BF<sub>4</sub>]<sup>−</sup>·CO<sub>2</sub> = −21.55; [Tf<sub>2</sub>N]<sup>−</sup>·H<sub>2</sub>S = −25.63; [PF<sub>6</sub>]<sup>−</sup>·H<sub>2</sub>S = −27.29; [BF<sub>4</sub>]<sup>−</sup>·H<sub>2</sub>S = −34.91, all in kJ/mol) and it is inversely correlated to the solubility. Nevertheless, the interaction strength between ion pairs obtained for the C<sub>1</sub>mim-anion series shows the following order: [C<sub>1</sub>mim][Tf<sub>2</sub>N] < [C<sub>1</sub>mim][PF<sub>6</sub>] < [C<sub>1</sub>mim][BF<sub>4</sub>], with binding energy above −300 kJ/mol. The high solubility exhibited by CO<sub>2</sub> in [C<sub>4</sub>mim][Tf<sub>2</sub>N] is related to the weakening of electrostatic interaction, due to the higher charge distribution of the anion, which is bulkier.<sup>8</sup> This relation was determined by Fernandes et al.<sup>65</sup> and suggests that, for this case, the entropic component, as described posteriorly, is more significant for the gases solubility.

**Dispersion Effects.** The [C<sub>*n*</sub>mim][Tf<sub>2</sub>N] series was studied considering C<sub>*n*</sub>mim from [C<sub>1</sub>mim]<sup>+</sup> to [C<sub>8</sub>mim]<sup>+</sup>, except for [C<sub>3</sub>mim]<sup>+</sup>, at B3LYP and M06-2X/6-311+G\*\* levels of theory. The optimized geometries at M06-2X for the [C<sub>1</sub>mim][Tf<sub>2</sub>N], [C<sub>4</sub>mim][Tf<sub>2</sub>N], and [C<sub>8</sub>mim][Tf<sub>2</sub>N] ion pairs are described in Figure 14. The results from quantum chemistry calculations are given in Table 8. Some optimized systems at B3LYP are summarized in Figure S5, in the Supporting Information.

As can be observed in Figure 14, the main interactions occur between oxygen from [Tf<sub>2</sub>N]<sup>−</sup> and, at least, three hydrogen atoms from the cation, including from the methyl group, bonded to the C=N and −CH<sub>2</sub> groups. The minor intermolecular distance O···H was found in the O···H(C=N) interaction site, the stronger interaction of the ion pair, with a partial charge of 0.307 $e$  in [C<sub>1</sub>mim][Tf<sub>2</sub>N].

The increasing alkyl chain is accompanied by an increase of the ion volume, promoting charge distribution to a greater extent. So, it is expected that the cation will be more stable and interaction with the anion weaker, according to the binding energy data. At B3LYP, the binding energy for [C<sub>1</sub>mim][Tf<sub>2</sub>N] is −327.21 kJ/mol with  $d_{\text{min}}$  = 2.012 Å. For [C<sub>8</sub>mim][Tf<sub>2</sub>N],  $\Delta E_{\text{CP}}$  = −313.41 kJ/mol and  $d_{\text{min}}$  = 2.223 Å. Considering the M06-2X results, the decline of the interaction strength is noted only from [C<sub>4</sub>mim][Tf<sub>2</sub>N] to [C<sub>8</sub>mim][Tf<sub>2</sub>N], with −365.85

and −351.89 kJ/mol, respectively, where dispersion forces are more significant. This effect has been associated with solubility. Gonzalez-Miquel et al.<sup>28</sup> measured solubility and diffusion coefficients for CO<sub>2</sub> in [C<sub>6</sub>mim][Tf<sub>2</sub>N], [C<sub>8</sub>mim][Tf<sub>2</sub>N], and [C<sub>10</sub>mim][Tf<sub>2</sub>N], at  $T$  = 298.15, 308.15, and 323.15 K at 20 bar. The researchers found that the solubility increases with alkyl chain, following the order: [C<sub>10</sub>mim]<sup>+</sup> > [C<sub>8</sub>mim]<sup>+</sup> > [C<sub>6</sub>mim]<sup>+</sup>. On the other hand, the diffusivity decreases with the alkyl chain, temperature, and pressure. For [C<sub>6</sub>mim][Tf<sub>2</sub>N], the diffusion coefficient is  $6.24 \times 10^{-11}$  m<sup>2</sup>/s, while [C<sub>10</sub>mim][Tf<sub>2</sub>N] has  $4.06 \times 10^{-11}$  m<sup>2</sup>/s. The explanation is that there is an occurrence of weakening of the cation–anion interaction, generating an increase of free volume in the IL, which provides higher space to accommodate gases. This effect is related to entropic contribution to solubility.<sup>66</sup> The free volume availability is associated with the elevated solubility of H<sub>2</sub>S in [C<sub>2</sub>mim][Tf<sub>2</sub>N] compared to [C<sub>2</sub>mim][PF<sub>6</sub>].<sup>67</sup> At 333.15 K, the Henry's law constant is 2.45 and 3.74 MPa, respectively. In this sense, Costa et al.<sup>35</sup> observed through MD simulations of [C<sub>2</sub>mim][Tf<sub>2</sub>N] that the free volume does not have an important role in the capacity of carrying out CO<sub>2</sub> in the IL, due to the increase of the fractional free volume and free volume in comparison to concentration. However, we need to emphasize that the energetic also has an important role in the explanation about solubility.

Data referred to ion pairs with cations from ether-functionalized imidazolium based ionic liquids are described in Table 9. [C<sub>1</sub>Odmim][Tf<sub>2</sub>N] can be compared to [C<sub>3</sub>mim][Tf<sub>2</sub>N], where the oxygen is bonded to the imidazolium ring through the −CH<sub>2</sub> group. [C<sub>3</sub>mim][Tf<sub>2</sub>N] has minor affinity between cation–anion, with  $\Delta E_{\text{CP}}$  = −318.49 kJ/mol, while [C<sub>1</sub>Odmim][Tf<sub>2</sub>N] presents  $\Delta E_{\text{CP}}$  = −331.44 kJ/mol. Analogously, [C<sub>1</sub>Oemim][Tf<sub>2</sub>N] is compared to [C<sub>4</sub>mim][Tf<sub>2</sub>N], with higher affinity,  $\Delta E_{\text{CP}}$  = −323.77 kJ/mol at the B3LYP level.

Similar to [C<sub>6</sub>mim][Tf<sub>2</sub>N], the [C<sub>1</sub>OC<sub>2</sub>Odmim][Tf<sub>2</sub>N] and the [C<sub>1</sub>OC<sub>2</sub>Oemim][Tf<sub>2</sub>N] ion pairs showed higher affinity, with  $\Delta E_{\text{CP}}$  = −325.60 and −326.07 kJ/mol, respectively, at B3LYP, and −386.50 kJ/mol along with −380.32 kJ/mol at M06-2X. For [C<sub>6</sub>mim][Tf<sub>2</sub>N],  $\Delta E_{\text{CP}}$  = −363.18 kJ/mol (M06-2X) and −317.81 kJ/mol (B3LYP). Panels A and B of Figure 15 highlight the partial charges for these systems.

Considering the isolated [C<sub>6</sub>mim]<sup>+</sup>, the carbon atom bonded to nitrogen in the imidazolium ring is almost neutral, with partial charge of −0.060 $e$ , and hydrogen 0.215 $e$ . The same carbon in [C<sub>1</sub>OC<sub>2</sub>Oemim]<sup>+</sup> presents −0.099 $e$ . The introduction of an ether group promotes a charge redistribution in atoms from the alkyl chain, reducing the negative charge in atoms away from the

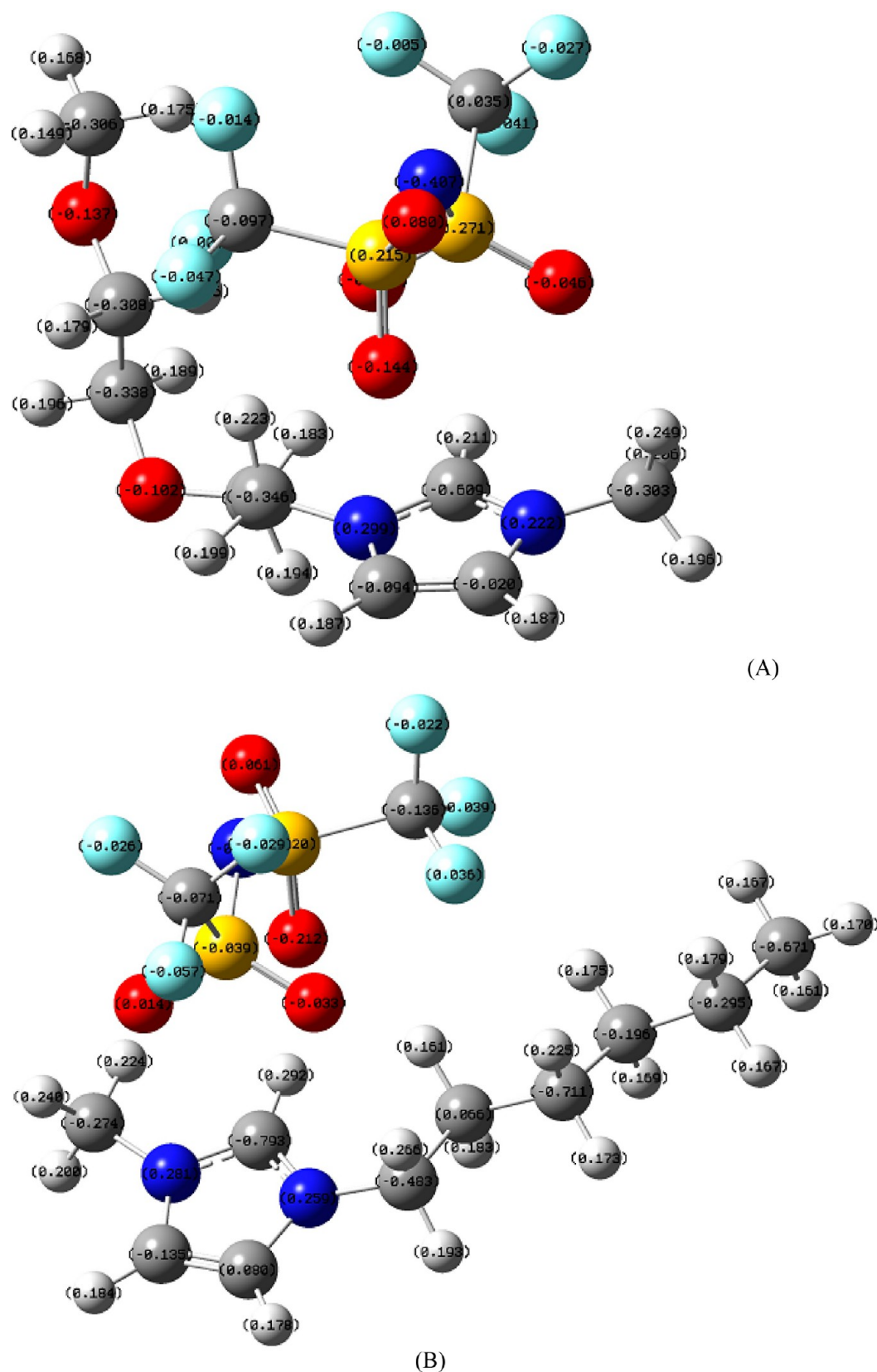


**Figure 15.** Schematic representation for partial charges determined for  $[\text{C}_1\text{OC}_2\text{Oemim}][\text{Tf}_2\text{N}]$  (A) and  $[\text{C}_6\text{mim}][\text{Tf}_2\text{N}]$  (B) at M06-2X/6-311+G\*\*. The gray, red, dark blue, light blue, yellow, and white spheres represent carbon, oxygen, nitrogen, fluorine, sulfur, and hydrogen atoms, respectively.

ring, due to its higher electronegativity. As an example, the last and antepenult carbon in  $[\text{C}_6\text{mim}]^+$  have partial charges of  $-0.656e$  and  $-0.421e$ , respectively, while in  $[\text{C}_1\text{OC}_2\text{Oemim}]^+$

the same carbons have  $-0.216e$  and  $-0.314e$ . After interaction with the anion, the charge over the carbon bonded to nitrogen in the ring reaches  $-0.793e$ , resulting from the charge transfer,

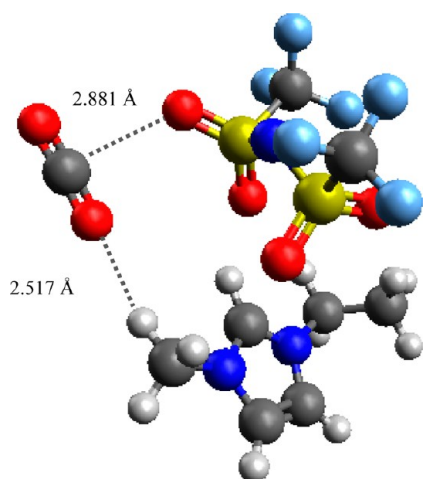


**Figure 16.** Schematic representation for  $[\text{C}_2\text{mim}][\text{Tf}_2\text{N}]$  optimized geometry, at the B3LYP/6-311+G\*\* level of theory. The gray, red, dark blue, light blue, yellow, and white spheres represent carbon, oxygen, nitrogen, fluorine, sulfur, and hydrogen atoms, respectively.

while hydrogen becomes more positive ( $0.292e$ ). In this site, the interaction is weaker in  $[\text{C}_1\text{OC}_2\text{Oemim}][\text{Tf}_2\text{N}]$ , with charges of  $-0.609e$  and  $0.211e$  for C and H, respectively. In view of the alkyl chain, the first carbon presents a partial charge of  $-0.483e$  in  $[\text{C}_6\text{mim}][\text{Tf}_2\text{N}]$ , while the second one is more positive, with  $0.066e$ . The charges from the hydrogen atoms decline with distance from imidazolium ring, for the two cases, with  $0.266e$  (HC bonded to N) and  $0.161e$  (H from *n*-hexyl chain), for  $[\text{C}_6\text{mim}][\text{Tf}_2\text{N}]$ . The last carbon from the alkyl chain has a partial charge of  $-0.671e$  and  $0.306e$  for  $[\text{C}_6\text{mim}][\text{Tf}_2\text{N}]$  and  $[\text{C}_1\text{OC}_2\text{Oemim}][\text{Tf}_2\text{N}]$ , respectively. Therefore, we can observe that this charge redistribution is responsible for stronger interactions in imidazolium-functionalized cations compared to nonfunctionalized ones and it also noted in imidazolium-gas interactions, but not in this extent.

**Ion Pairs $\cdots\text{CO}_2$ .** After studying the interactions between ion pairs, we allocated  $\text{CO}_2$  near the structure optimized previously. It was considered about four configurations with frozen ion pair from  $[\text{C}_3\text{mim}][\text{Tf}_2\text{N}]\cdots\text{CO}_2$ , since that gas cannot modify its structure. The  $[\text{C}_4\text{mim}][\text{Tf}_2\text{N}]$  system presented similar organization to that as shown in Figure 16. Data related to  $\text{SO}_2$  are

given in Table S7 (Supporting Information) and the same behavior is expected considering  $\text{SO}_2$  and  $\text{H}_2\text{S}$ .

Both systems have exhibited an alkyl chain curvature, what modified the  $[\text{Tf}_2\text{N}]^-$  conformation and, consequently, the interaction site with gas. Other systems have configurations similar to Figure 16. Table 10 describes the results obtained at B3LYP and M06-2X (in parentheses) levels of theory, considering  $\text{CO}_2$ .  $\Delta E_{\text{CPT}}$  represents the total binding energy, taking into account the anion–cation interaction. The exclusion of this interaction is done in  $\Delta E_{\text{CPG}}$ , which represents the interaction between gas and the ion pair. As cited by Chen et al., the binding energy reflects the interaction strength between IL and gas, as well as gas stabilization through interactions. The negative values for the binding energies indicate that systems have the tendency to be stable with gas absorption.<sup>27</sup>

In Table 10, we can observe that the C–O bond length (from gas) diverges from the isolated one of  $1.161 \text{ \AA}$ . As an example, for  $[\text{C}_6\text{mim}][\text{Tf}_2\text{N}]$ ,  $d_1 = 1.158 \text{ \AA}$  and  $d_2 = 1.164 \text{ \AA}$ . Such a difference was noted for cation–gas systems, which present  $d_1 = 1.153 \text{ \AA}$  and  $d_2$  about  $1.169 \text{ \AA}$ , for all  $\text{CO}_2$ -cation systems. On the other hand, OCO angle deviates from the linear geometry, as observed for the anion- $\text{CO}_2$  systems, for example,  $[\text{Tf}_2\text{N}]^-\cdots\text{CO}_2$  has  $\text{OCO} = 175.8^\circ$ . For comparison,  $\text{OCO} = 180.0^\circ$  for  $[\text{C}_1\text{mim}]^+\cdots\text{CO}_2$ , and  $d_1 = d_2 = 1.161 \text{ \AA}$  for  $[\text{Tf}_2\text{N}]^-\cdots\text{CO}_2$ . This fact suggests that the gas interacts with the cation and the anion, simultaneously, as expected. Figure 17 shows partial charges for  $[\text{C}_2\text{mim}][\text{Tf}_2\text{N}]\cdots\text{CO}_2$ . The  $\text{O}\cdots\text{H}$  (gas- $[\text{C}_2\text{mim}]^+$ ) interaction site is evidenced with the charge transfer between these atoms.

In Figure 17, O exhibit partial charge of  $-0.232e$  (isolated gas is  $-0.186e$ ), while hydrogen, of  $0.209e$ . The charge transfer anion–gas is suggested in the (anion)  $\text{O}\cdots\text{C}$  interaction, with carbon charge of  $0.491e$ , in contrast to  $0.372e$  presented by isolated  $\text{CO}_2$ . For isolated  $[\text{Tf}_2\text{N}]^-$ , the charge is slightly higher,  $-0.141e$ .

In Table 10, we can note the fluctuation of the binding energies with the alkyl chain, but the interaction between gas and ion pair exhibits an interesting behavior, considering the B3LYP methodology. The gas pair interaction presents an increasing strength with the alkyl chain, except for  $[\text{C}_6\text{mim}][\text{Tf}_2\text{N}]$ , with  $-10.64 \text{ kJ/mol}$ , while  $\Delta E_{\text{CPG}}$  is  $-10.30 \text{ kJ/mol}$  for  $[\text{C}_1\text{mim}][\text{Tf}_2\text{N}]$  and  $-25.48 \text{ kJ/mol}$  for  $[\text{C}_4\text{mim}][\text{Tf}_2\text{N}]$ . Taking into account the M06-2X methodology, the behavior is the opposite, with decay until  $[\text{C}_4\text{mim}][\text{Tf}_2\text{N}]$ , but an increase is observed from  $[\text{C}_4\text{mim}][\text{Tf}_2\text{N}]$  to  $[\text{C}_8\text{mim}][\text{Tf}_2\text{N}]$ , with  $\Delta E_{\text{CPG}}$  of  $-20.63$

**Table 10.** Data Obtained from Electronic Structure Calculations for  $[\text{C}_n\text{mim}][\text{Tf}_2\text{N}]$  Systems with  $\text{CO}_2$ , at the B3LYP/6-311+G\*\* Level of Theory<sup>a</sup>

system	$E_0+\text{ZPE}$ (hartrees)	total $\Delta E_{\text{CPT}}$ (kJ/mol)	gas–ion pair $\Delta E_{\text{CPG}}$ (kJ/mol)	$d_1$ (Å)	$d_2$ (Å)	OCO angle (deg)
$[\text{C}_1\text{mim}][\text{Tf}_2\text{N}]\cdots\text{CO}_2$	−2321.487310	−337.51 (−394.90)	−10.30 (−29.50)	1.158	1.164	177.6
$[\text{C}_2\text{mim}][\text{Tf}_2\text{N}]\cdots\text{CO}_2$	−2360.786795	−331.78	−10.64	1.157	1.165	177.3
$[\text{C}_3\text{mim}][\text{Tf}_2\text{N}]\cdots\text{CO}_2$	−2400.082077	−342.70 (−388.27)	−24.21 (−25.09)	1.157	1.165	177.8
$[\text{C}_4\text{mim}][\text{Tf}_2\text{N}]\cdots\text{CO}_2$	−2439.378829	−343.25 (−386.48)	−25.48 (−20.63)	1.157	1.165	177.8
$[\text{C}_6\text{mim}][\text{Tf}_2\text{N}]\cdots\text{CO}_2$	−2517.971977	−328.45 (−328.53)	−10.64 (−25.27)	1.158	1.164	177.4
$[\text{C}_8\text{mim}][\text{Tf}_2\text{N}]\cdots\text{CO}_2$	−2596.562870	−326.06 (−377.55)	−12.65 (−25.66)	1.158	1.164	177.3

<sup>a</sup>Data in parentheses are relative to the M06-2X/6-311+G\*\* level of theory. The columns describe electronic energy with ZPE correction ( $E_0+\text{ZPE}$ ), binding energies with BSSE correction ( $\Delta E_{\text{CPT}}$  and  $\Delta E_{\text{CPG}}$ ), in which  $\Delta E_{\text{CPT}}$  include the interaction between cation and anion, while  $\Delta E_{\text{CPG}}$  does not.  $d_1$  and  $d_2$  are the  $\text{CO}_2$  bond lengths and the angle is exhibited in the last column.

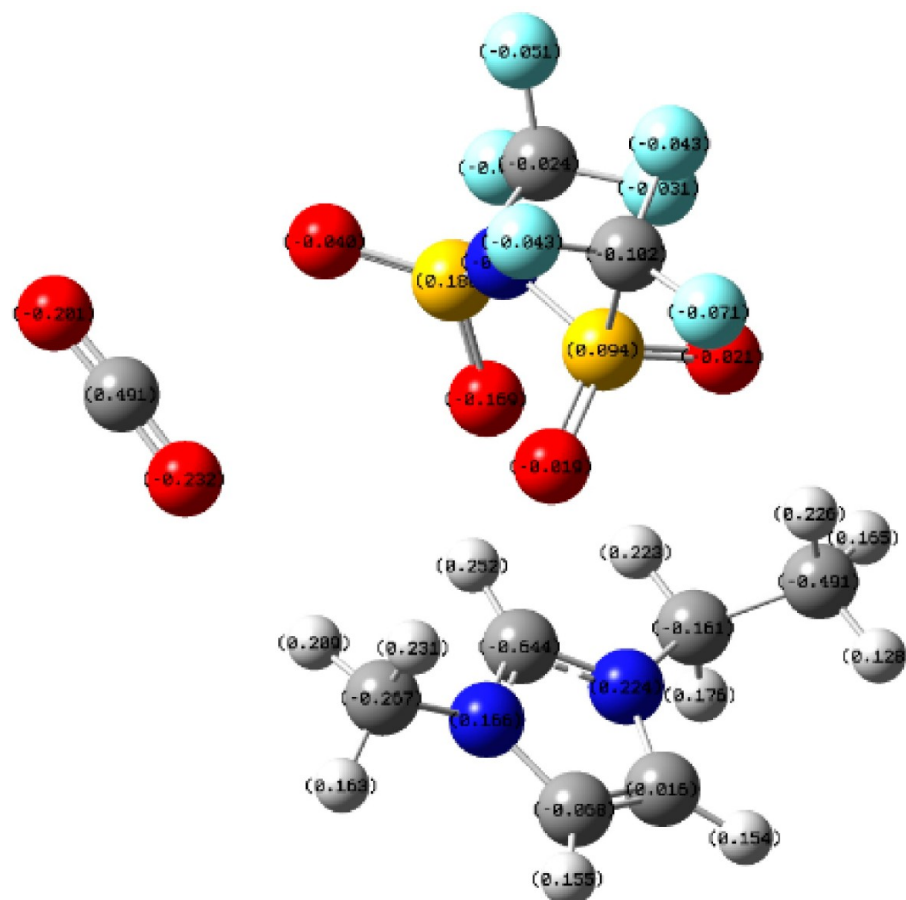


**Figure 17.** Schematic representation for the partial charges calculated for  $[\text{C}_2\text{mim}][\text{Tf}_2\text{N}]\text{CO}_2$  at the B3LYP/6-311+G\*\* level. The gray, red, dark blue, light blue, yellow, and white spheres represent carbon, oxygen, nitrogen, fluorine, sulfur, and hydrogen atoms, respectively.

and  $-25.66$  kJ/mol. This fact was verified for the ion pairs without gas and suggests that from  $[\text{C}_4\text{mim}][\text{Tf}_2\text{N}]$ , M06-2X agreed with B3LYP. As expected, this behavior is shown by  $\text{SO}_2$ -ion pair interactions (Table S7, Supporting Information), which also present stronger interactions than  $\text{CO}_2$ .

In this sense, it is important to note that the interaction strength between  $[\text{C}_n\text{mim}]$  cation–gas becomes higher with the alkyl chain variation.  $\Delta E_{\text{CP}} = -16.25$  and  $-13.84$  kJ/mol for  $[\text{C}_1\text{mim}]^+-\text{CO}_2$  and  $[\text{C}_8\text{mim}]^+-\text{CO}_2$ , with slight increase in  $[\text{C}_6\text{mim}]^+-\text{CO}_2$ , of  $-14.77$  kJ/mol, compared to  $[\text{C}_4\text{mim}]^+-\text{CO}_2$ . Therefore, it is possible to conclude that the weakening of the cation–anion interaction makes the anion more available to interact with gas. In accordance with this, Xu et al.<sup>68</sup> describe that the cation–anion interaction weakening is a form to enhance basicity, mainly IL considered have the same anion, for example,  $[\text{Tf}_2\text{N}]^-$ . Considering that the interactions of acid–base type are weaker than covalent ones, the electrostatic interaction exercises the first role in intermolecular acid–base interactions. Taking into consideration the statements made above, we have developed a novel structure: for this, we have chosen a cation with low acidity and anion with intermediate basicity, resulting in the  $[\text{THA}][\text{Tf}_2\text{N}]$  system, with optimized geometry described in Figure 18.

As expected, this structure shows a weak affinity between cation–anion, with binding energy of  $-274.86$  kJ/mol (value with BSSE corrected). This ion pair has a bulky cation, where the three oxygen atoms from the anion show interaction with hydrogen atoms bonded near the charge center. This structure exhibits

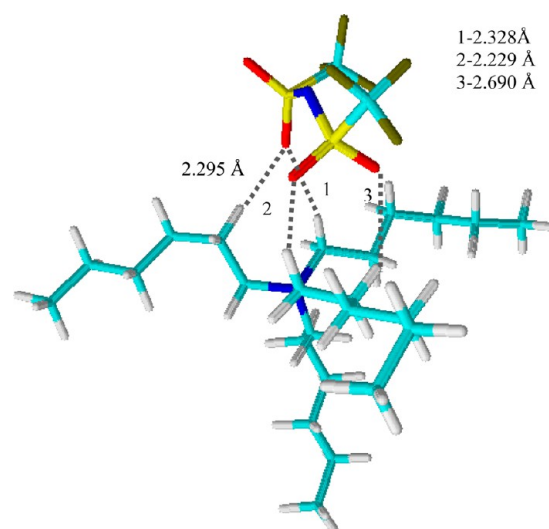


**Figure 18.** Schematic representation of the  $[\text{THA}][\text{Tf}_2\text{N}]$  optimized geometry at the B3LYP/6-311+G\*\* level of theory. The gray, red, dark blue, light blue, yellow, and white colors represent carbon, oxygen, nitrogen, fluorine, sulfur, and hydrogen atoms, respectively.

less interaction strength in comparison to  $[\text{C}_8\text{mim}][\text{Tf}_2\text{N}]$  and  $[\text{C}_4\text{mim}][\text{B}(\text{CN})_4]$ , with calculated binding energies of  $-313.41$  and  $-283.63$  kJ/mol, respectively. Systems containing that  $[\text{B}(\text{CN})_4]$  anion have been reported in recent papers, and are considered promising for  $\text{CO}_2$  capture applications, with high



solubility and selectivity.<sup>69–71</sup> At the MP2/6-31G level of theory, this binding energy  $[\text{C}_4\text{mim}][\text{B}(\text{CN})_4]$  is equal to  $-315.84$  kJ/mol.<sup>71</sup> Then, we expect  $[\text{THA}][\text{TF}_2\text{N}]$  presents higher space to accommodate gases and we are investigating these systems to a greater extent, through MD simulations in the condensed phase.

## CONCLUSIONS

In this contribution, ab initio calculations were performed at the B3LYP/M06-2X levels of theory considering ion–gas and ionic pairs interactions. In accordance with reported results, anion–gas interactions are stronger than cation–gas ones, taking into account  $\text{CO}_2$ ,  $\text{SO}_2$ , and  $\text{H}_2\text{S}$  gases. Among the studied systems,  $[\text{THA}]^+$  and  $[\text{FAP}]^-$  had the lowest affinity with gases, while  $[\text{phosphonium}]^+$  and  $[\text{acetate}]^-$  ions had the highest. As a consequence of the Lewis acid–base interaction, the gas angle suffers a deviation after interaction for cation– $\text{SO}_2$  and anion–gas systems, while a stretching in the C–O and S–O bond distances was observed resulting from the cation–gas interactions. The higher interaction strengths found for  $\text{SO}_2$  systems were associated with the higher polarizability, in accordance with Pearson's theory.

In the second step, we verified that the effect of the anion exchange is more pronounced than cation exchange in the binding energy results. The  $\text{C}_n\text{mim-Tf}_2\text{N}$  series exhibited a binding energy decreasing with an increase of the alkyl chain, at B3LYP. At M06-2X, the results are in accordance with those from  $[\text{C}_4\text{mim}][\text{TF}_2\text{N}]$ , and this allows us to conclude that this method is more efficient in the description of systems with the alkyl chain more extended. This weakening of the cation–anion interaction has been associated with the higher availability of free volume and increasing of the solubility with alkyl chain. Then it suggests the cation–anion interaction strength is responsible for generating voids in the ionic liquid structure, accommodating the gases better. Therefore, the interactions between cation–anion in the ion pair are the most important to evaluate the solubility, considering the magnitude of the binding energy values in comparison to anion–gas and cation–gas ones, which are approximately ten times lower. In this sense, the calculations including  $\text{CO}_2$  in the imidazolium-based ionic liquids suggest that the anion is more available to interact with gas when cation–anion interaction becomes weaker.

We have analyzed unpublished systems with imidazolium-functionalized cations and  $[\text{THA}][\text{TF}_2\text{N}]$ . The binding energy results proved higher in comparison with the common imidazolium series. The  $[\text{THA}][\text{TF}_2\text{N}]$  ion pair shows promise from an energetic point of view, taking into account the lower affinity in comparison with  $[\text{C}_8\text{mim}][\text{TF}_2\text{N}]$  and  $[\text{C}_4\text{mim}][\text{B}(\text{CN})_4]$ .

## ASSOCIATED CONTENT

### Supporting Information

Tables S1–S2: binding energies for cation–gas and anion–gas interactions; Tables S3–S4: data from AIM analysis over BCP and RCP for anion–gas interactions; Table S5: frequencies of in-plane and out-of-plane bending modes of  $\text{CO}_2$ , with deviation between these modes; Table S6: data relative to the frontier orbitals of gases; Figure S1: optimized geometries for cation–gas interactions; Figure S2: geometries of the critical points for some gas–anion interactions; Figure S3: relation between OCO angle and binding energy of the anion– $\text{CO}_2$  interactions; Figure S4: relation between stretching mode and H–S deviation after interaction with anion; Figure S5: optimized geometries of some ion pairs at B3LYP; and Table S7: data obtained from electronic structure calculations for  $[\text{C}_n\text{mim}][\text{TF}_2\text{N}]$  systems with  $\text{SO}_2$ .

This material is available free of charge via the Internet at <http://pubs.acs.org>.

## AUTHOR INFORMATION

### Corresponding Author

\*E-mail: [ltcosta@id.uff.br](mailto:ltcosta@id.uff.br). Tel: +55 21 26292157. Fax: +55 21 26292166.

### Notes

The authors declare no competing financial interest.

## ACKNOWLEDGMENTS

This work was supported by the FAPEMIG, specifically by the project APQ-01120-10. We would also like to thank CAPES for the fellowship given to Giane B. Damas. We are grateful to Maurício Silva, Anna Carolina Octaviani, and Tuanan Lourenço.

## REFERENCES

- (1) Hester, R. E.; Harrison, R. M. *Issues in Environmental Science and Technology: Carbon Capture and Storage*; The Royal Society of Chemistry: London, UK, 2010.
- (2) Ramdin, M.; Loos, T. W.; Vlugt, T. J. H. State-of-the-Art of  $\text{CO}_2$  Capture with Ionic Liquids. *Ind. Eng. Chem. Res.* **2012**, *51* (24), 8149–8177.
- (3) Cadena, C.; Anthony, J. L.; Shah, J. K.; Morrow, T. I.; Brennecke, J. F.; Maginn, E. J. *J. Am. Chem. Soc.* **2004**, *126* (16), 5300–5308.
- (4) Blanchard, L. A.; Gu, Z.; Brennecke, J. F. High-Pressure Phase Behavior of Ionic Liquid/ $\text{CO}_2$  Systems. *J. Phys. Chem. B* **2001**, *105* (12), 2437–2444.
- (5) Gurkan, B.; Goodrich, B. F.; Mindrup, E. M.; Ficke, L. E.; Massel, M.; Seo, S.; Senftle, T. P.; Wu, H.; Glaser, M. F.; Shah, J. K.; et al. Molecular Design of High Capacity, Low Viscosity, Chemically Tunable Ionic Liquids for  $\text{CO}_2$  Capture. *J. Phys. Chem. Lett.* **2010**, *1* (24), 3494–3499.
- (6) Stevanovic, S.; Podgorsek, A.; Padua, A. A. H.; Gomes, M. F. C. Effect of Water on the Carbon Dioxide Absorption by 1-Alkyl-3-methylimidazolium Acetate Ionic Liquids. *J. Phys. Chem. B* **2012**, *116* (49), 14416–14425.
- (7) Almantariotis, D.; Stevanovic, S.; Fandino, O.; Pensado, A. S. Absorption of Carbon Dioxide, Nitrous Oxide, Ethane and Nitrogen by 1-Alkyl-3-methylimidazolium ( $\text{C}_n\text{mim}$ ,  $n=2,4,6$ ). *J. Phys. Chem. B* **2012**, *116* (26), 7728–7738.
- (8) Jalili, A. H.; Safavi, M.; Ghotbi, C.; Mehdizadeh, A.; Hosseini-Jenab, M.; Taghikani, V. Solubility of  $\text{CO}_2$ ,  $\text{H}_2\text{S}$ , and their Mixture in the Ionic Liquid 1-Octyl-3-Methylimidazolium Bis(Trifluoromethyl)-Sulfonylimide. *J. Phys. Chem. B* **2012**, *116* (9), 2758–2774.
- (9) Blath, J.; Christ, M.; Deubler, N.; Hirth, T.; Schiestel, T. Gas Solubilities in Room Temperature Ionic liquids- Correlation Between RTIL-Molar Mass and Henry's Law Constant. *Chem. Eng. Journal* **2011**, *172* (1), 167–176.
- (10) Yokozeki, A.; Shiflett, M. B.; Junk, C. P.; Grieco, L. M.; Foo, T. Physical and Chemical Absorptions of Carbon Dioxide in Room-Temperature Ionic Liquids. *J. Phys. Chem. B* **2008**, *112* (S1), 16654–16663.
- (11) Zhang, T. Q.; Sweeney, B.; Kim, H.; Lee, B. K. Characterizing the Parameter Space of Complex Self-Assembly Reactions Through Quantitative Discrete Event Simulations. *Biophys. J.* **2007**, *0*, 533A–534A.
- (12) Zhang, X.; Liu, Z.; Wang, W. Screening of Ionic Liquids to Capture  $\text{CO}_2$  by COSMO-RS and Experiments. *AIChE J.* **2008**, *54* (10), 2717–2728.
- (13) Maginn, E. J. Molecular Simulation of Ionic Liquids: Current Status and Future Opportunities. *J. Phys.: Condens. Matter* **2009**, *21* (37), 373101–373118.
- (14) Bhargava, B. L.; Balasubramanian, S. Probing Anion-Carbon Dioxide Interactions in Room Temperature Ionic Liquids: Gas phase Cluster Calculations. *Chem. Phys. Lett.* **2007**, *444* (4), 242–246.

- (15) Ghobadi, A.; Taghikhani, V.; Elliott, J. R. Investigation on the Solubility of SO<sub>2</sub> and CO<sub>2</sub> in Imidazolium-Based Ionic Liquids Using NPT Monte Carlo Simulation. *J. Phys. Chem. B* **2011**, *115* (49), 13599–13607.
- (16) Shimoyama, Y.; Ito, A. Predictions of Cation and Anion Effects on Solubilities, Selectivities and Permeabilities for CO<sub>2</sub> in Ionic Liquid Using COSMO Based Activity. *Fluid Phase Equilib.* **2010**, *296* (2), 178–182.
- (17) Maiti, A. Atomistic Modeling Toward High-Efficiency Carbon Capture: A Brief Survey with A Few Illustrative Examples. *Int. J. Quantum Chem.* **2014**, *114* (3), 163–175.
- (18) Gurkan, B. E.; de la Fuente, J. C.; Mindrup, E. M.; Ficke, L. E.; Goodrich, B. F.; Price, E. A.; Schneider, W. F.; Brennecke, J. F. Equimolar CO<sub>2</sub> Absorption by Anion-Functionalized Ionic Liquids. *J. Am. Chem. Soc.* **2010**, *132* (7), 2116–2117.
- (19) Bhargava, B. L.; Saharay, M.; Balasubramanian, S. Ab Initio Studies on [bmim][PF<sub>6</sub>]-CO<sub>2</sub> mixture and CO<sub>2</sub>. *Bull. Mater. Sci.* **2008**, *31* (3), 327–334.
- (20) Sumida, K.; Rogow, D. L.; Mason, J. A.; McDonald, T. M.; Bloch, E. D.; Herm, Z. R.; Bae, T.-H.; Long, J. R. Carbon Dioxide Capture in Metal-Organic Frameworks. *Chem. Rev.* **2012**, *112* (2), 724–781.
- (21) Luis, P.; Gerven, T. V.; der Bruggen, B. V. Recent Developments in Membrane-Based Technologies for CO<sub>2</sub> Capture. *Prog. Energy Combust. Sci.* **2012**, *38* (3), 419–448.
- (22) Welton, T. Room Temperature Ionic Liquids. Solvents for Synthesis and Catalysis. *Chem. Rev.* **1999**, *99* (8), 2071–2084.
- (23) Hough, W. L.; Smiglak, M.; Rodriguez, H.; Swatoski, R. P.; Spear, S. K.; Daly, D. T.; Pernak, J.; Grisell, J. E.; Carliss, R. D.; Soutullo, M. D.; et al. The Third Evolution of Ionic Liquids: Active Pharmaceutical Ingredients. *New J. Chem.* **2007**, *31*, 1429–1436.
- (24) Costa, L. T.; Ribeiro, M. C. C. Molecular Dynamics Simulation of Polymer Electrolytes based on Poly (Ethylene Oxide) and Ionic Liquids. I. Structural Properties. *J. Chem. Phys.* **2006**, *124* (18), 184902–184910.
- (25) Costa, L. T.; Ribeiro, M. C. C. Molecular Dynamics Simulation of Polymer Electrolytes based on Poly(ethylene Oxide) and Ionic Liquids. II. Dynamical Properties. *J. Chem. Phys.* **2007**, *127* (16), 164901–164909.
- (26) Costa, L. T.; Siqueira, L. J. A.; Nicolau, B. G.; Ribeiro, M. C. C. Raman Spectra of Olymer Electrolytes Based on Poly (Ethylene Glycol) Dimethyl Ether, Lithium Perchlorate, and the Ionic Liquid 1-Butyl-3-Methylimidazolium Hexafluorophosphate. *Vib. Spectrosc.* **2010**, *54* (2), 155–158.
- (27) Chen, J.; Li, W. W.; Yu, H. Q. Capture of H<sub>2</sub>S from Binary Gas Mixture by Imidazolium-Based Ionic Liquids with Nonfluorous Anions: A Theoretical Study. *AIChE J.* **2013**, *59* (10), 3824–3833.
- (28) Gonzalez-Miquel, M.; Bedia, J.; Rodriguez, F. Solubility and Diffusivity of CO<sub>2</sub> in [hxmm][NTf<sub>2</sub>], [omim][NTf<sub>2</sub>], and [dcmim][NTf<sub>2</sub>] at T = (298.15, 308.15, and 323.15) K and Pressures up to 20 bar. *J. Chem. Eng. Data* **2014**, *59* (2), 212–217.
- (29) Sudha, S. Y.; Khanna, A. Evaluating the Interactions of CO<sub>2</sub>-Ionic Liquid Systems through Molecular Modeling. *World Acad. Sci., Eng. Technol.* **2009**, *57*, 539–542.
- (30) Pennline, H. W.; Luebke, D. R.; Jones, K. L.; Myers, C. R.; Morsi, B. I.; Heintz, Y. J.; Ilconich, J. B. Progress in Carbon Dioxide Capture and Separation Research for Gasification-Based Power Generation Point Sources. *Fuel Proc. Technol.* **2008**, *89* (9), 897–907.
- (31) Raveendran, P.; Wallen, S. L. Cooperative C-H...O Hydrogen Bonding in CO<sub>2</sub>-Lewis Base Complexes: Implications for Solvation in Supercritical CO<sub>2</sub>. *J. Am. Chem. Soc.* **2002**, *124* (42), 12590–12599.
- (32) Rogers, R. D.; Seddon, K. R. Ionic Liquids IIIB: Transformations and Process. *ACS Symp. Ser.* **2005**, *902*, i–vii.
- (33) Bara, J. E.; Carlisle, T. K.; Gabriel, C. J.; Camper, D.; Finotello, A.; Gin, D. L.; Noble, R. D. Guide to CO<sub>2</sub> Separations in Imidazolium-Based Room-Temperature Ionic Liquids. *Ind. Eng. Chem. Res.* **2009**, *48* (6), 2739–2751.
- (34) Siqueira, L. J. A.; Ribeiro, M. C. C. Alkoxy Chain Effect on the Viscosity of a Quaternary Ammonium Ionic Liquid: Molecular Dynamics Simulations. *J. Phys. Chem. B* **2009**, *113* (4), 1074–1079.
- (35) Lourenço, T. C.; Coelho, M. F.; Ramalho, T. C.; Spoel, D. v. d.; Costa, L. T. Insights on the Solubility of CO<sub>2</sub> in 1-Ethyl-3-methylimidazolium Bis (trifluoro) sulphonylimide from the Microscopic Point of View. *Environ. Sci. Technol.* **2013**, *47* (13), 7421–7429.
- (36) Hanwell, M. D.; Curtis, D. E.; Lonie, D. C.; Vandermeersch, T. Avogadro: An Advanced Semantic Chemical Editor, Visualization and Analysis Platform. *J. Cheminform.* **2012**, *4*, 1–17.
- (37) Becke, A. D. Density-Functional Thermochemistry. III. The Role of Exact Exchange. *J. Chem. Phys.* **1993**, *98* (7), 5648–5652.
- (38) Ditchfield, R.; Hehre, W. J.; Pople, J. A. Self-Consistent Molecular-Orbital Methods IX. An Extended Gaussian-Type Basis for Molecular-Orbital Studies of Organic Molecules. *J. Chem. Phys.* **1971**, *54*, 724–728.
- (39) Lagrost, C.; Gmouh, S.; Vaultier, M.; Hapiot, P. Specific Effects of Room Temperature Ionic Liquids on Cleavage Reactivity: Example of the Carbon-Halogen Bond Breaking in Aromatic Radical Anions. *J. Phys. Chem. A* **2004**, *108* (29), 6175–6182.
- (40) Talaty, E. R.; Raja, S.; Storhaug, V. J.; Daulle, A. Carper, W. R. Raman and Infrared Spectra and ab Initio Calculations of C2–4MIM Imidazolium Hexafluorophosphate Ionic Liquids. *J. Phys. Chem. B* **2004**, *108* (35), 13177–13184.
- (41) Yu, G.; Zhang, S.; Yao, X.; Zhang, J.; Dong, K.; Dai, W.; Mori, R. Design of Task-Specific Ionic Liquids for Capturing CO<sub>2</sub>: A Molecular Orbital Study. *Ind. Eng. Chem. Res.* **2006**, *45* (8), 2875–2880.
- (42) Zahn, S.; MacFarlane, D. R.; Izgorodina, E. I. Assessment of Kohn–Sham Density Functional Theory and Møller–Plesset Perturbation Theory for Ionic Liquids. *Phys. Chem. Chem. Phys.* **2013**, *15* (32), 13664–13675.
- (43) Zhao, Y.; Truhlar, D. The M06 Suite of Density Functionals for Main Group Thermochemistry, Thermochemical Kinetics, Noncovalent Interactions, Excited States, And Transition Elements: Two New Functionals And Systematic Testing of Four M06-Class Functionals And 12 Other Functionals. *Theor. Chem. Acc.* **2008**, *120*, 215–241.
- (44) Dennington, R.; Keith, T.; Millam, J. *GaussView*, Version 5; Semichem Inc.: Shawnee Mission, KS, 2009.
- (45) Frisch, M. J. *Gaussian 09*; Gaussian, Inc.: Wallingford, CT, 2009.
- (46) Keith, T. A. *AIMAll*, Version 13.05.06; TK Gristmill Software: Overland Park, KS, 2013.
- (47) Bader, R. F. W. *Atoms in Molecules: A Quantum Theory*, 2nd ed.; Oxford University Press: Oxford, UK, 1994.
- (48) Koch, W.; Holthausen, M. C. *A Chemist's Guide to Density Functional Theory*; Wiley-VCH: Weinheim, Germany, 2001.
- (49) Oliveira, B. G.; Araújo, R. C.; Ramos, M. N. The QTAIM Molecular Topology and The Quantum-Mechanical Description of Hydrogen Bonds and Dihydrogen Bonds. *Quim. Nova* **2010**, *33* (5), 1155–1162.
- (50) Matta, C. F.; Boyd, R. J. *The Quantum Theory of Atoms in Molecules: From Solid State to DNA and Drug Design*, 1st ed.; Wiley-VCH: Weinheim, Germany, 2007.
- (51) Popelier, P. L. A. Characterization of a Dihydrogen Bond on the Basis of the Electron Density. *J. Phys. Chem. A* **1998**, *102* (10), 1873–1878.
- (52) Viswanathan, B. Reflections on the Electrochemical Reduction of Carbon Dioxide on Metallic Surfaces. *Indian J. Chem.* **2012**, *51A*, 166–173.
- (53) Grabowski, S. J. Non-covalent interactions – QTAIM and NBO analysis. *J. Mol. Model.* **2013**, *19* (11), 4713–4721.
- (54) Carvalho, P. J.; Álvarez, V. H.; Schröder, B.; Gil, A. M.; Marrucho, I. M.; Aznar, M.; Santos, L. M. N. B. F.; Coutinho, J. A. Specific Solvation Interactions of CO<sub>2</sub> on Acetate and Trifluoroacetate Imidazolium Based Ionic Liquids at High Pressures. *J. Phys. Chem. B* **2009**, *113* (19), 6803–6812.
- (55) Zhang, S.; Sun, N.; He, X.; Lu, X.; Zhang, X. Physical Properties of Ionic Liquids: Database and Evaluation. *J. Phys. Chem. Ref. Data* **2006**, *35* (4), 1475–1516.
- (56) Zhao, Z.; Dong, H.; Zhang, X. The Research Progress of CO<sub>2</sub> Capture with Ionic Liquids. *Chin. J. Chem. Eng.* **2012**, *20* (1), 120–129.

- (57) Bhargava, B. L.; Krishna, A. C.; Balasubramanian, S. Molecular Dynamics Simulations Studies of CO<sub>2</sub>-[bmim][PF<sub>6</sub>] Solutions: Effect of CO<sub>2</sub> Concentration. *AIChE J.* **2008**, *54* (11), 2971–2978.
- (58) Shimanouchi, T. *Tables of Molecular Vibrational Frequencies Consolidated*; National Bureau of Standards: Washington, DC, 1972; Vol I.
- (59) Herzberg, G. *Electronic Spectra and Electronic Structure of Polyatomic Molecules*; Van Nostrand: New York, NY, 1966.
- (60) Pearson, R. G. Hard and Soft Acids and Bases- The Evolution of A Chemical Concept. *Coord. Chem. Rev.* **1990**, *100*, 403–425.
- (61) Vasconcellos, M. L. A. A. Pearson's Theory for Organic Chemistry Courses: a Practical and Theoretical Exercise Applied in the Classroom. *Quim. Nova* **2014**, *37* (1), 171–175.
- (62) Lide, D. R. *Handbook of Chemistry and Physics*, 84th ed.; CRC Press: Boca Raton, FL, 2003–2004.
- (63) Anthony, J. L.; Anderson, J. L.; Maginn, E. J.; Brennecke, J. F. Anion Effects on Gas Solubility in Ionic Liquids. *J. Phys. Chem. B* **2005**, *109* (13), 6366–6374.
- (64) Weingärtner, H. Understanding Ionic Liquids at the Molecular Level: Facts, Problems and Controversies. *Angew. Chem., Int. Ed.* **2008**, *47* (4), 654–670.
- (65) Fernandes, A. M.; Rocha, M. A.; Freire, M. G.; Marrucho, I. S.; Coutinho, J. A. P.; Santos, L. M. N. B. F. Evaluation of Cation-Anion Interaction Strength in Ionic Liquids. *J. Phys. Chem. B* **2011**, *115* (14), 4033–4041.
- (66) Hong, S. Y.; Im, J.; Palgunadi, J.; Lee, S. D.; Lee, J. S.; Kim, H. S.; Cheong, M.; Jung, K. D. Ether-Functionalized Ionic Liquids as Highly Efficient SO<sub>2</sub> Absorbents. *Energy Environ. Sci.* **2011**, *4*, 1802–1806.
- (67) Sakhaeinia, H.; Jalili, A. H.; Taghikani, V.; Sakefordi, A. A. Solubility of H<sub>2</sub>S in Ionic Liquids 1-Ethyl-3-Methylimidazolium Hexafluorophosphate ([emim][PF<sub>6</sub>]) and 1-Ethyl-3-Methylimidazolium Bis(trifluoromethyl)sulfonylimide ([emim][Tf<sub>2</sub>N]). *J. Chem. Eng. Data* **2010**, *55* (12), 5839–5845.
- (68) Xu, D.; Yang, Q.; Su, B.; Bao, Z.; Ren, Q.; Xing, H. Enhancing the Basicity of Ionic Liquids by Tuning the Cation-Anion Strategy and via the Anion-Tethered Strategy. *J. Phys. Chem. B* **2014**, *118* (4), 1071–1079.
- (69) Mahuin, S.; Lee, J. S.; Baker, G. A.; Luo, H.; Dai, S. High CO<sub>2</sub> Solubility, Permeability and Selectivity in Ionic Liquids with the Tetracyanoborate Anion. *J. Membr. Sci.* **2010**, *353* (1), 177–183.
- (70) Mahurin, S. M.; Hillesheim, P. C.; Yeary, J. S.; Jiang, D.; Dai, S. Performance of Nitrile-Containing Anions in Task-Specific Ionic Liquids for Improved CO<sub>2</sub>/N<sub>2</sub> Separation. *RSC Adv.* **2012**, *2* (1), 11813–11819.
- (71) Gupta, K. M.; Jiang, J. Systematic Investigation of Nitrile Based Ionic Liquids for CO<sub>2</sub> Capture: A Combination of Molecular Simulation and Ab Initio Calculation. *J. Phys. Chem. C* **2014**, *118* (6), 3110–3118.